Contributions of human long-wave and middle-wave cones to motion detection

C. F. Stromeyer III, R. E. Kronauer, A. Ryu, A. Chaparro and Rhea T. Eskew Jr*

*Division of Applied Sciences and Department of Psychology, Harvard University, Cambridge, MA 02138 and *Department of Psychology, Northeastern University, Boston, MA 02115, USA*

1. It has been suggested that motion may be best detected by the luminance mechanism. If this is the most sensitive mechanism, motion thresholds may be used to isolate the luminance mechanism and study its properties.

2. A moving (1 cycle deg^{-1}), vertical, heterochromatic (red-plus-green), foveal grating was presented on a bright yellow (577 nm wavelength) field. Detection and motion (direction identification: left *versus* right) thresholds were measured for different amplitude ratios of the red and green components spatially summed in phase or in antiphase. Threshold contours plotted in cone-contrast co-ordinates (L', M') for the long-wave (L) and middle-wave (M) cones, revealed two motion mechanisms: a luminance mechanism that responds to a weighted sum of L and M contrasts, and a spectrally opponent mechanism that responds to a weighted difference.

3. Detection and motion thresholds, measured at 1–4 Hz, were identical for luminance gratings, having equal cone contrasts, L' and M', of the same sign. For chromatic gratings, with L' and M' of opposite sign, motion thresholds were higher than detection thresholds. A red–green hue mechanism may mediate chromatic detection, and a separate spectrally opponent motion mechanism may mediate motion.

4. The red–green hue mechanism was assessed from 1 to 15 Hz with an explicit hue criterion. The detection contour had a constant slope of one, implying equal L' and M' contributions of opposite sign. For motion identification, L' and M' contributed equally at 1 Hz, but the M' contribution was attenuated at higher velocities.

5. The cone-contrast metric provides a physiologically relevant comparison of sensitivities of the two motion mechanisms. At 1 Hz, the spectrally opponent motion mechanism is ~4 times more sensitive than the luminance mechanism. As temporal frequency is increased, the relative sensitivities change so that the luminance mechanism is more sensitive above 9 Hz.

6. The less sensitive motion mechanism was isolated with a quadrature phase protocol, using a pair of heterochromatic red-plus-green gratings, counterphase flickering in spatial and temporal quadrature phase with respect to each other. One grating was set slightly suprathreshold and oriented in cone contrast (L', M') so as to potentiate a single motion mechanism, the sensitivity of which was probed with the second grating, which was varied in (L', M'). This allowed us to measure the motion detection contour of the less sensitive luminance mechanism at low velocities. At low velocities the luminance mechanism was strongly affected by L cone contrast, but at high velocities the L and M cones contributed more equally. These changing cone weights were observed with both luminance flicker and motion.

7. Phase shifts between L and M cone signals within the two motion mechanisms were measured by varying the relative temporal phase of the two flickering gratings. Only small phase shifts were found in the spectrally opponent motion mechanism measured at 4 and 6 Hz (essentially no phase shifts were observed in the red–green hue mechanism). Within the luminance mechanism, the L signal lags M by as much as 30 deg at 4–9 Hz, and by a lesser amount at lower frequencies; at 21 Hz there is little phase shift. These large phase shifts may reflect properties of the phasic retinal ganglion cells. Such large phase shifts imply that moving chromatic gratings, when suprathreshold, will directly stimulate the luminance mechanism.

In human vision it has been suggested that motion is portrayed by luminance signals, with purely colour-varying patterns conveying little sense of motion (Ramachandran & Gregory, 1978; Livingstone & Hubel, 1987). Motion may appear to be strongly (and non-veridically) slowed for coloured patterns at equiluminance (Moreland, 1982; Cavanagh, Tyler & Favreau, 1984). The perceived motion of such equiluminant patterns may be particularly impaired outside the fovea (Lindsey & Teller, 1990). Moreover, adding a colour variation to a luminance pattern may act to inhibit the perception of motion (Cavanagh & Favreau, 1985).

We asked whether the detection of motion *per se* provides a clear method for isolating the luminance pathway and studying its properties. Thresholds for identifying the direction of motion of a low spatial frequency, foveal grating were measured over a wide range of velocities. The heterochromatic (red-plus-green) grating, presented against a bright yellow background, stimulates the long-wave (L) and middle-wave (M) cones in a ratio determined by the relative amplitude of the red and green components. At each velocity, motion thresholds were measured for many red-to-green amplitude ratios. The motion thresholds are plotted as detection contours in two-dimensional co-ordinates of L cone contrast *versus* M cone contrast (Stromeyer, Cole & Kronauer, 1985, 1987). Different segments of the contours suggest the presence of a luminance and a spectrally opponent motion mechanism that respond, respectively, to the sum and the difference of the L and M cone-contrast signals. The cone-contrast co-ordinates allow a physiologically relevant comparison of sensitivities of the two mechanisms.

We developed several protocols to separate the two motion mechanisms and to determine better the L and M contributions and their relative temporal phases within each mechanism. To isolate each motion mechanism, we used a pair of counterphase flickering (contrast-reversing) gratings. Each counterphase pattern is drift balanced, consisting of two, matched, left- and right-moving, sine-wave gratings. The spectral composition (red and green) of one counterphase pattern is adjusted to stimulate weakly one motion mechanism, while producing little stimulation in the other. This pattern potentiates the stimulated mechanism, making it sensitive to the differential (left *versus* right) motion imparted by adding a second counterphase pattern in spatial–temporal quadrature phase with the first (Stromeyer, Kronauer, Madsen & Klein, 1984). The second pattern produces motion only to the extent that it stimulates the potentiated mechanism, thus allowing us to distinguish the two motion mechanisms even when one is considerably more sensitive than the other. We can thereby measure the detection contour of the less sensitive mechanism. With a similar protocol we assessed the L *versus* M signal phase shifts within both motion mechanisms, thus further differentiating the mechanisms.

Parts of this work have been presented at several meetings (Stromeyer, Eskew & Kronauer, 1990; Stromeyer, Eskew, Ryu & Kronauer, 1991*b*).

METHODS

Stimuli and calibration

A vertical, heterochromatic (red-plus-green), sine-wave grating of 1 cycle deg^{-1} was presented on a bright adapting field. The field appeared as a yellow disc (4·2 deg diameter uniform background) with a central whitish area (3·5 deg grating region), containing superposed red, green and violet light (from three cathode ray tube (CRT) monitors). The illuminance of the grating area was ~3300 td, metameric with 577 nm (disregarding the short-wave (S) cones). For one observer, A.C., the field was 580 nm. There was a black fixation point in the centre of the field.

Red and green gratings were summed spatially in phase or in antiphase. By adjusting the amplitude ratio of the two gratings, we obtained a stimulus representing any desired vector (Fig. 1) in the L and M cone-contrast co-ordinates ($L' = \Delta L/L$, $M' = \Delta M/M$). In the definition of M cone contrast, for example, ΔM represents the amplitude (maximal excursion) of the M cone quantal catch owing to the spatially varying component of the grating, and M represents the mean M cone quantal catch owing to all steady light components in the field. The grating is specified by its vector angle in cone contrast co-ordinates, $\tan^{-1}(M'/L')$, and by its vector length, $\mathrm{VL} = (L'^2 + M'^2)^{1/2}$. Two stimuli were used: a simple red-plus-green grating that moved at a uniform velocity left or right, or a pair of red-plus-green gratings presented in counterphase flicker at the same rate.

Gratings were generated with an Innisfree Image Synthesizer and were displayed on three Tektronix 608 monitors with different phosphors. The custom-made Synthesizer had two grating modules but only one spatial frequency generator, thus assuring that the pair of flickering gratings were matched in spatial frequency. Each of the two grating signals was converted to a heterochromatic (red-plus-green) grating with control circuits that split each grating signal into two separate signals, for the red and green CRTs, respectively. Contrast was controlled by 12-bit digital-to-analog converters (used with ×10 attenuators at low contrasts). The contrast of each CRT was linear with voltage up to ~35% contrast, as calibrated with 1 cycle deg^{-1} square-wave gratings.

The apparatus was modified from Lee & Stromeyer (1989). Stimuli were viewed monocularly, through an artificial pupil mounted on an achromatizing lens (Powell, 1981) that corrects for ocular chromatic aberration. The pupil subtended 3 mm at the eye. The observer was positioned by means of a dental impression on a rigid x-y-z translator. The adapting field (in Maxwellian view) was produced with a 50 W halogen lamp, filtered with a narrow-band interference filter. The Maxwellian lens focused the beam on the artificial pupil. The three CRTs, each placed 51 cm from the eye, were optically combined with dichroic mirrors, and joined with the adapting field by a beam-

splitter cube which attenuated the light from the CRTs by 20%. Before each session, the observer viewed in-phase, red and green, square-wave gratings, and, if necessary, made a tiny adjustment of the raster position until the gratings appeared coincident. The rasters occupied a relatively uniform area of the CRTs of about 16 cm^2.

The CRT phosphors decayed to one-tenth intensity in <1·2 ms and the frame rate was 106·2 Hz. The slow (x-axis) sweeps of the red and green rasters were coincident on the *retina*, providing the precise temporal synchrony needed for the phase measurements. We examined the light modulation of two 1 mm points, one on the red CRT and one on the green CRT, that were coincident on the retina, using two photodiodes and a dual beam oscilloscope with single time base. Any asynchrony was <1 deg phase.

Radiance calibrations were made at the eyepiece with a calibrated United Detector Technology Pin-10 photodiode and 101B amplifier. Spectral calibrations were made over the range 350–750 nm, with a monochromator (2 nm half-bandwidth (HBW)). The resultant spectral radiance curves were weighted by the cone spectra (Smith & Pokorny, 1975) to calculate the cone contrasts. Mean radiance of all lights was measured each session with a calibrated radiometer.

Stimuli had the following spectral properties. The main adapting field was yellow (578 nm wavelength, 10 nm HBW), with superposed light from the violet, green and red CRTs. The violet CRT was filtered with a 460 nm short-pass filter, producing light of 441 nm (centroid) and 8·8 log quanta deg s^{-1}, which served to reduce sensitivity of the S cones to the green grating. The green CRT was filtered with a Schott DG530 glass filter that removed light below 515 nm (which would otherwise be absorbed by the macular pigment and thereby produce a spatially non-uniform grating) and reduced stimulation of the S cones. The red CRT was filtered with a 640 nm short-pass filter (to remove infrared for calibration purposes) and a Schott RG610 filter, producing two narrow bands at 617 and 626 nm.

Stimuli

The stimulus was a moving grating or a pair of counterphase flickering gratings. Each grating had a specified vector angle in cone-contrast space (L', M'). For simplicity, first consider a luminance grating. The luminance profile of a vertical moving grating is represented by

$$B(x,t) = B_0[1 + m\cos(2\pi fx \pm 2\pi\omega t)],$$

where B_0 is mean luminance, m is grating contrast, f is spatial frequency, and ω is temporal frequency.

Counterphase gratings were used with a quadrature phase protocol (Stromeyer *et al.* 1984). A fixed-contrast, suprathreshold grating serves as a 'pedestal'; it sinusoidally reverses contrast, producing a standing wave with no net motion left or right,

$$B(x,t) = B_0[1 + 2m'\cos(2\pi fx)\cos(2\pi\omega t)].$$

This pattern can be decomposed into two matched gratings, moving at equal rates in opposite directions, with contrast

$$m_{\text{left}} = m_{\text{right}} = m'.$$

A variable-contrast, counterphase 'test' grating of the same spatial and temporal frequency is added to the pedestal in spatial–temporal quadrature phase (shifted in phase by 90 deg in space and time relative to the pedestal). The expression for the test-plus-pedestal is

$$B(x,t) = B_0[1 + 2m'\cos(2\pi fx)\cos(2\pi\omega t) + 2\Delta\sin(2\pi fx)\sin(2\pi\omega t)],$$

with the cosine terms representing the pedestal and the sine terms representing the quadrature test (with contrast 2Δ). This expression can be rewritten as,

$$B(x,t) = B_0[1 + (m_{\text{left}} - \Delta)\cos(2\pi fx + 2\pi\omega t) + (m_{\text{right}} + \Delta)\cos(2\pi fx - 2\pi\omega t)],$$

indicating that the test increases the contrast of the right component of the pedestal by +Δ and decreases the left component by an equivalent amount, −Δ. Thus the test imparts differential motion to the standing-wave pedestal, which by itself has no net motion. Motion is reversed by inverting the test temporal phase. By selecting the appropriate red and green composition, the pedestal can be made to stimulate mostly one spectral mechanism only. Tests added to this pedestal can create a motion signal only to the extent that the test and pedestal stimulate a common spectral mechanism.

Threshold determination

Thresholds were measured with a forced-choice staircase: each trial had two temporal intervals, signalled by tones, and separated by 100 ms. The pattern was presented in one interval chosen randomly: the contrast was ramped on for 339 ms with a raised cosine, held constant for 678 ms and then ramped off. (The envelope was expanded twofold at 1 Hz.) Thresholds were measured for detection (choosing the interval with the test pattern) or for identifying the direction of motion (left or right). In the quadrature protocol, only direction thresholds were measured, with a single test interval. Test contrast was lowered by 0·10 log unit after two successive correct responses and increased by the same amount after each error, estimating the 71%-correct detection level (Wetherill, 1963). Tones provided response feedback. The first two contrast reversals were discarded, and the next four to six reversals were saved. Several staircases were randomly interleaved in a run; each threshold was typically based on four to twelve staircases over several runs. To measure the detection contours, a single test vector angle was used in each run, with the angle changed randomly between runs. In one experiment (Fig. 8) observers set thresholds using an explicit hue citerion and the method of adjustment. The contrast was increased 0·10 log units when the moving grating was judged to have no apparent red–green hue and it was similarly decreased when the grating was judged to be coloured; the threshold was based on approximately fifty staircase reversals. Volunteer observers had normal colour vision, and the study was approved by the university ethics committee.

RESULTS

Moving gratings: detection and direction identification

Thresholds of the red-plus-green gratings are represented in cone-contrast co-ordinates (Fig. 1*A*); the vertical axis depicts M cone contrast and the horizontal axis, L cone contrast. Each grating is represented by a vector symmetric about the origin, since the grating modulation

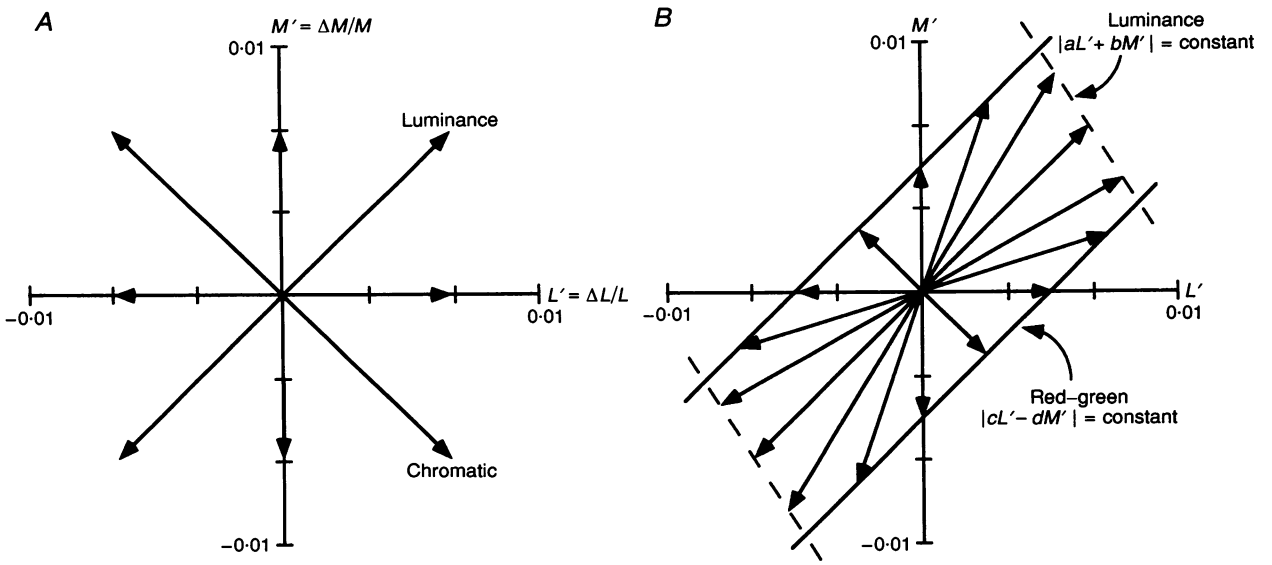

Figure 1. Test stimuli represented in L and M cone-contrast co-ordinates

A, each grating, comprised of a different red–green light ratio, is represented by a vector symmetric about the origin in the cone-contrast co-ordinates. *B*, hypothetical detection mechanisms indicated by 'detection contours', depicting the threshold loci for a wide array of test vectors. The luminance mechanism responds to the *sum* of weighted L and M contrast (dashed contours of negative slope), and the red–green hue mechanism responds to the *difference* of equally weighted L and M contrast (continuous contours of slope ~1·0).

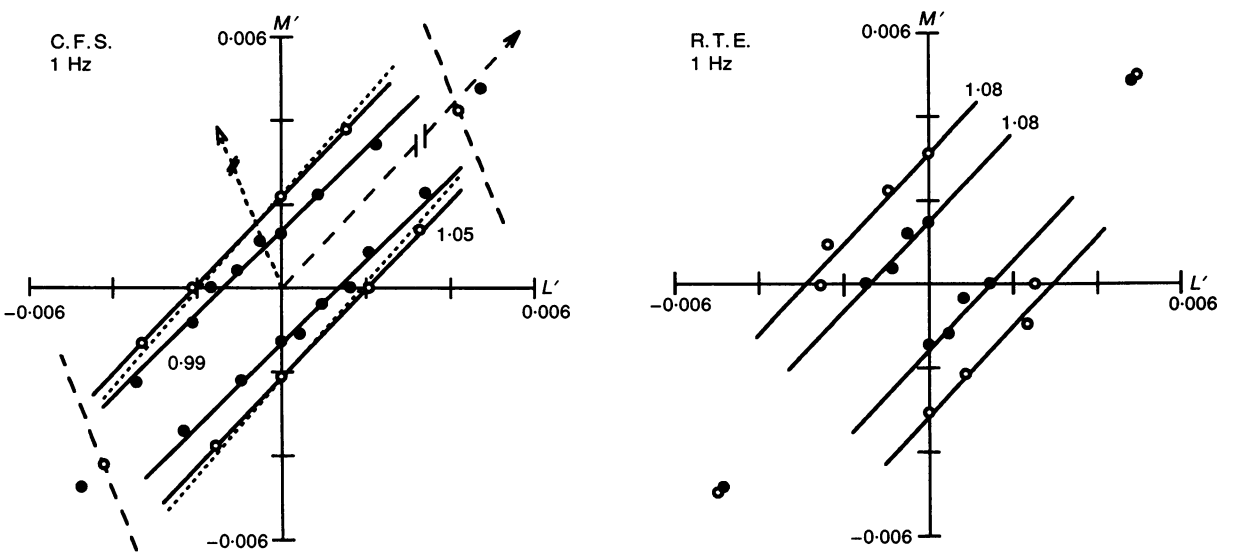

Figure 2. Detection (●) and direction identification (○) thresholds for a 1 cycle deg^{-1} grating (the spatial frequency always used) moving at 1 Hz, plotted in cone-contrast co-ordinates

Along the 45–225 deg luminance axis, detection and direction thresholds are similar; patterns may be detected by the LUM (luminance) mechanism which summates L and M contrasts. Remaining thresholds are fitted with continuous contours of slope ~1·0 (slopes designated beside contours), indicating that the L and M contrasts contribute with equal magnitude but with opposite sign to the RG (red–green) hue detection mechanism (●) and to the SPO (spectrally opponent) motion mechanism (○). The SPO motion mechanism is about 4 times more sensitive than the LUM mechanism. The dashed vectors (pedestals) and contours, from the quadrature protocol (Fig. 9), show that the slope of the SPO motion mechanism (short-dashed contours) is similar when assessed with either simple moving gratings or the quadrature protocol; only the latter protocol reveals the slope of the less sensitive LUM motion mechanism (long-dashed contours).

was symmetric about the mean adapting level. A 45–225 deg vector represents a luminance grating that modulated the L and M cones equally: as the grating moved past a point on the retina, the L and M cones were modulated sinusoidally in phase. A 135–315 deg vector represents a chromatic grating (not necessarily equiluminant) that equally modulated the L and M cones in antiphase. A vertical vector modulated M cones alone (the L cones are 'silenced'), while a horizontal vector modulated L cones alone.

Thresholds were measured for a wide array of vectors, and detection contours were fitted to the thresholds. Earlier results suggested that we could expect to see mechanisms with two distinct spectral signatures (Fig. 1*B*). The red–green chromatic mechanism (Thornton & Pugh, 1983; Stromeyer *et al.* 1985) responds to an *equally* weighted difference of L and M cone-contrast, $|cL' - dM'|$, where $c = d$. At threshold $|cL' - dM'| =$ constant, so red–green detection thresholds should form lines of unit slope in (L', M') space (Fig. 1*B*). The luminance mechanism (Stromeyer *et al.* 1987) responds to a weighted sum of L and M cone-contrast, $|aL' + bM'|$, with coefficients a and b of the same sign, implying a negative slope (Fig. 1*B*). The slope of the detection contour provides an estimate of the relative L and M cone weights, a/b, as shown in Fig. 11*A*.

Motion at 1 Hz

Results were first considered for a low velocity for which the pattern of results was quite simple (Fig. 2). First consider thresholds for detecting (●) the mere presence of the moving gratings. The straight lines fitted to the data in the second and fourth quadrants indicate the red–green chromatic detection mechanism. The luminance grating on the 45–225 deg axis was detected at 0·4–0·5% luminance contrast (Michelson contrast, which is equal to L' or M'). Sensitivity to the chromatic grating (135–315 deg axis) is 7 times greater. This sevenfold ratio of chromatic to luminance sensitivity is similar to that of a foveal 1 deg, 200 ms spot on the yellow field (Cole, Stromeyer & Kronauer, 1990), although the overall sensitivity for the gratings is 3 times that for the spots.

Figure 2 also shows direction identification (left *versus* right) thresholds (○) for the same moving gratings. On the 45–225 deg luminance axis, motion was seen at the detection threshold, in agreement with Watson, Thompson, Murphy & Nachmias (1980). (This result was also confirmed later for faster motion of 2 and 4 Hz.) For the chromatic directions, motion was not seen until the grating was raised 1·6 and 2 times above detection threshold for observers C.F.S. and R.T.E., respectively. The continuous lines fitted to these direction thresholds have slopes near 1·0, closely matching the slope for chromatic detection. As shown later, with increasing velocity, the chromatic detection contour maintains its slope of ~1·0, whereas the motion contour steepens, indicating that chromatic detection and motion may be mediated by different mechanisms. We call the three putative mechanisms RG (red–green hue mechanism),

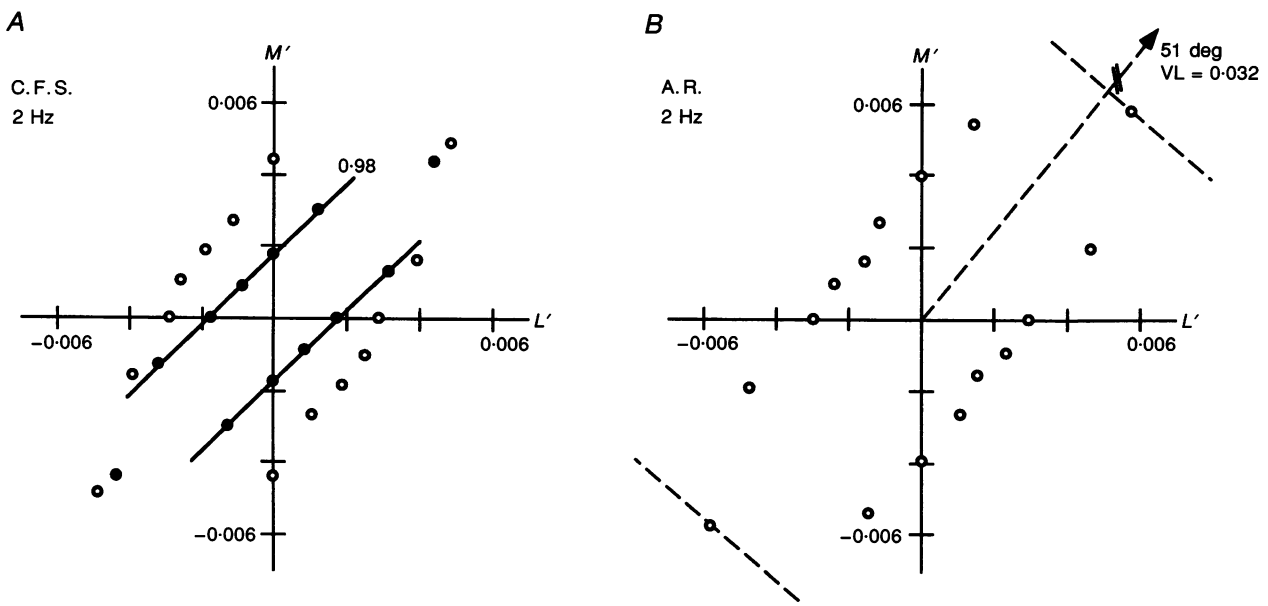

Figure 3. Detection (●) and direction identification thresholds (○) at 2 Hz

A, detection and direction thresholds are again similar along the luminance axis; other *detection* thresholds are fitted with a contour of slope ~1·0, reflecting the RG mechanism. The direction contours for SPO (second and fourth quadrants) are steeper – a tendency that increases with velocity, showing an L cone dominance. Dashed lines (*B*) indicate LUM slope assessed with quadrature protocol (the dashed vector represents the pedestal, and its cone-contrast angle and vector length, VL, are specified).

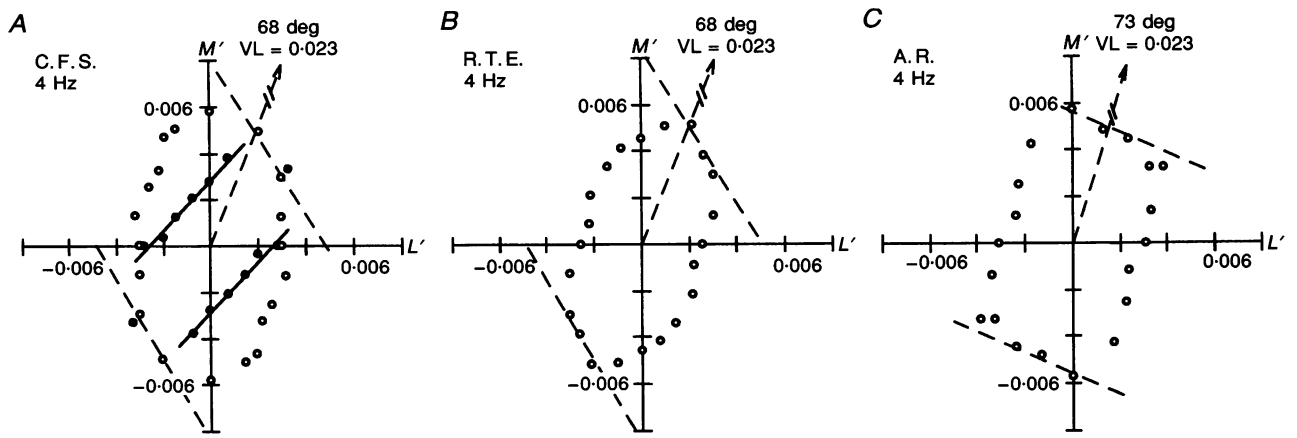

Figure 4. Detection (●) and direction identification thresholds (○) at 4 Hz

A, detection and direction thresholds are again similar along the luminance axis; the other detection thresholds reflect the RG hue mechanism. The SPO motion contours (○, second and fourth quadrants) are steeper than at lower velocities. Dashed contours indicate the LUM slope with the quadrature protocol. Contours measured with the quadrature protocol are expected to be straight and tangent to the direction contour for simple gratings at the point where the quadrature pedestal vector intersects the latter contours.

SPO (spectrally opponent motion mechanism), and LUM (luminance motion mechanism).

The LUM mechanism has low relative sensitivity at 1 Hz, and thus its detection contour cannot be determined by simple threshold measurements. The long- and short-dashed contours in Fig. 2 indicate the slope of the LUM and SPO contours, respectively, as assessed with the quadrature protocol, discussed later (in connection with Fig. 9).

Metha, Vingrys & Badcock (1994) recently reported foveal detection and direction identification contours at 1 Hz which have the same features as ours.

Direction identification at different velocities

Direction identification contours were measured for three observers at velocities of 2–21·2 Hz, as shown in Figs 3–7 (○). (Limited detection thresholds were obtained at 2 and 4 Hz, and these will be considered in the next section.) We first consider the qualitative features of the SPO motion

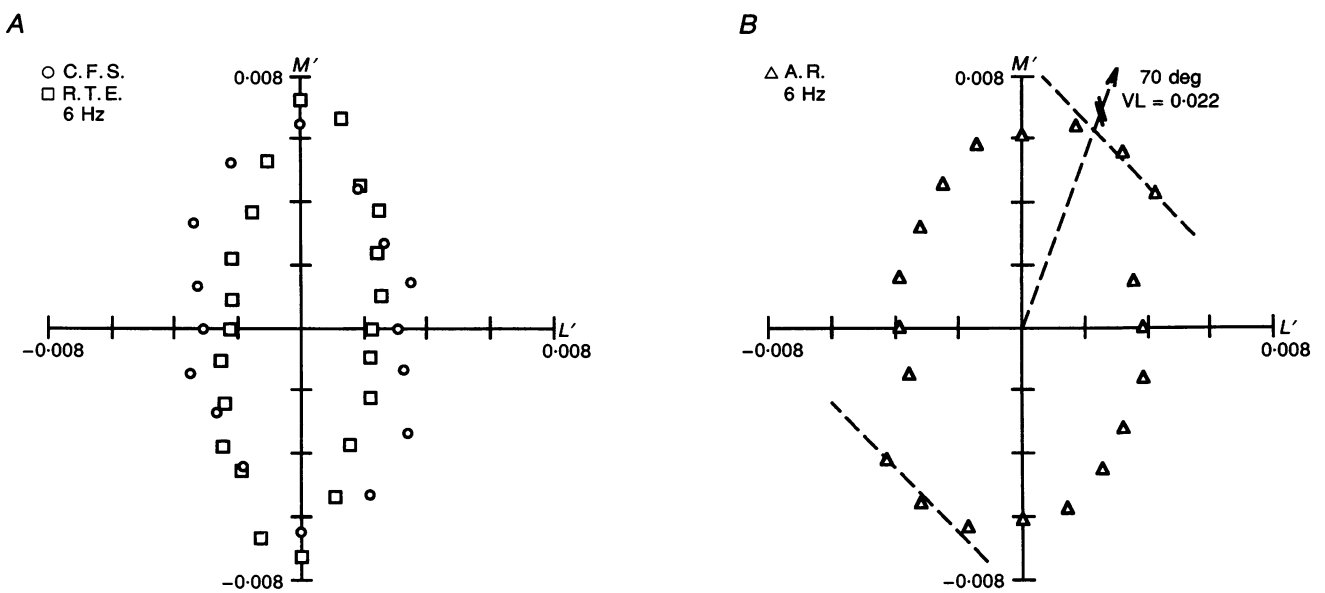

Figure 5. Direction identification thresholds at 6 Hz

Results for C.F.S. and R.T.E. are plotted together (*A*), and show higher SPO sensitivity for R.T.E. The SPO contours (second and fourth quadrants) are yet steeper at this higher velocity. Dashed contours (*B*) indicate the LUM slope with the quadrature protocol for observer A.R.

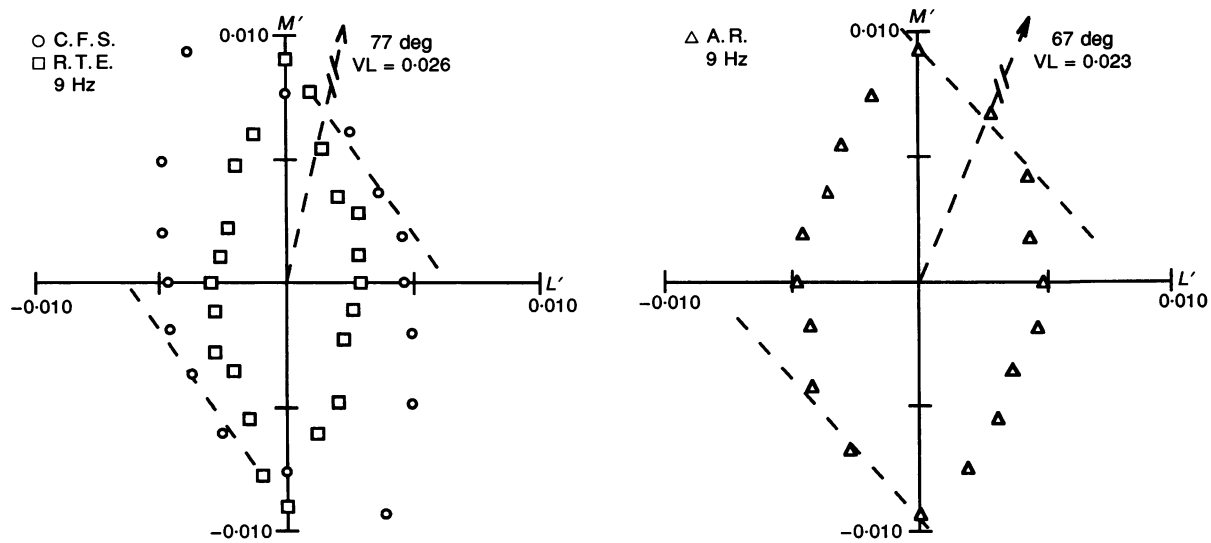

Figure 6. Direction identification thresholds at 9 Hz
For observers C.F.S. and A.R., the LUM slope was assessed with quadrature protocol (dashed contours).

mechanism. At 1 Hz this mechanism has a slope of ~1·0 (Fig. 2). As velocity is increased the SPO contour steepens, as shown by the thresholds within the second and fourth quadrants: at 2 Hz the slope is 1·3–1·5 (Fig. 3), at 4 Hz it is ~2 (Fig. 4), and at higher velocities (Figs 5–7) the slope is still steeper. This increased steepening above 4 Hz may be partly caused by the intervention of the LUM mechanism, which is more sensitive along the L than the M cone axis.

We next consider the LUM mechanism. This mechanism responds to a weighted sum of L' and M' and has a contour of negative slope. At 1 Hz the LUM mechanism can only be inferred from the one threshold measurement on the 45–225 deg axis where the detection and direction thresholds were very similar (Fig. 2). The LUM mechanism became more sensitive than the SPO mechanism when the velocity was raised to 9 Hz (Fig. 6), as seen by comparing the thresholds in quadrants 1 and 3 (for LUM) with thresholds in quadrants 2 and 4 (for SPO). At 15·2 Hz (Fig. 7*A*) the LUM mechanism is revealed by the data in the upper part of the first quadrant and lower third quadrant: the contours bend inward near the L cone axis, presumably because SPO intervenes. This inward bending is also seen at 17·7 Hz for R.T.E. (Fig. 7*B*), and is also weakly apparent in the results for C.F.S. and A.R., for whom there was insufficient test strength to measure complete contours. The LUM contour is best seen at 21·2 Hz (Fig. 7*C*) where the contours have a slope of approximately −1, indicating that L' and M' contribute about equally at high velocities. At low velocities the

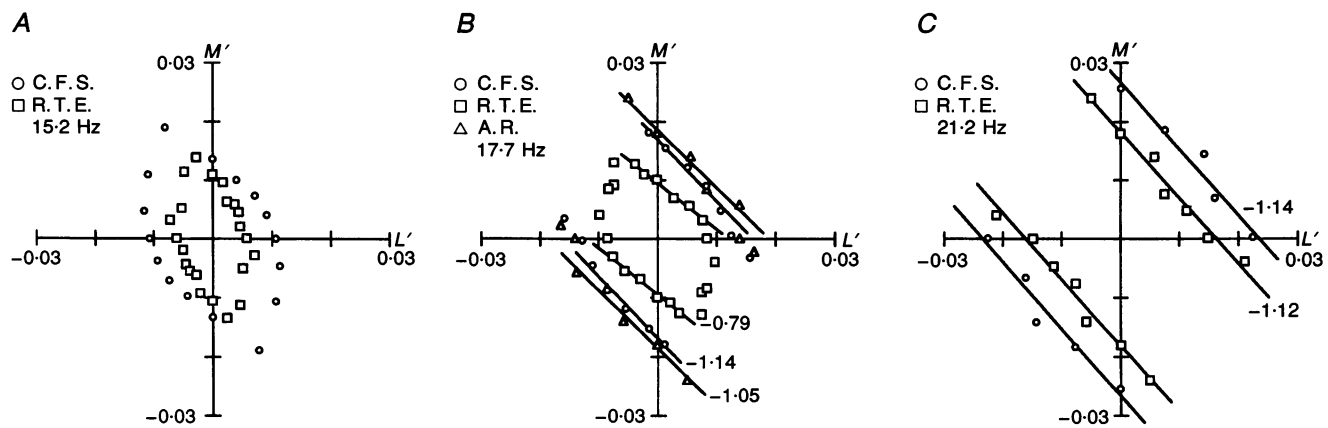

Figure 7. Direction identification thresholds at 15·2 (*A*), 17·7(*B*) and 21·2 Hz (*C*)
At higher velocities more of the LUM mechanism (continuous contours) is revealed, since SPO is less sensitive.

LUM contours are steeper, reflecting a relatively greater L cone contribution, a feature that will be seen better with the quadrature protocol. The dashed lines in Figs 3–6 are the LUM contours determined from the quadrature protocol (discussed later). The contours are drawn through data points tangent to the pedestal vector (dashed arrow), as explained later.

Detection thresholds and the red–green hue mechanism

In this section we consider further evidence that the RG hue mechanism may be distinct from the SPO motion mechanism. Figures 3*A* and 4*A* compare detection (●) and direction identification (○) thresholds for observer C. F. S. at 2 and 4 Hz, respectively. The chromatic detection thresholds are fitted by lines of slope of approximate value 1·0, indicating that L' and M' contribute with equal magnitude but with opposite sign to the RG mechanism. The direction thresholds in the second and fourth quadrants form steeper contours, indicating that the M cone signal is less effective for motion than for chromatic detection.

The method of adjustment, with an explicit hue criterion, was used to extend the RG measurements to higher velocities. The forced-choice method could not be used, since the observer might use a more sensitive motion mechanism to detect the gratings at certain vector angles. The contours without data points (Fig. 8) were obtained with the original forced-choice procedure (from Figs 2–4), whereas the contours with data points were obtained with the adjustment procedure. The adjustment procedure yields higher thresholds than the forced-choice procedure: the tail of the arrow (Fig. 8, left panel) indicates an adjustment threshold, while the tip represents a forced-choice threshold for the same test (which the observer felt appeared coloured but not moving at threshold). The present RG hue contours all have a slope of ~1·0, whereas the SPO motion contours (shown earlier) steepen above 1 Hz.

Additional evidence for separate RG and SPO mechanisms is provided by psychometric functions, measured at 4 Hz. Each grating was presented for a total of 500 forced-choice trials, at four or five 0·10 log unit contrast steps. Results were fitted by the Weibull function:

$$P(a) = 1 - (1/2)\exp[-a/\hat{a})^{E}],$$

where $P(a)$ is probability of correct response for stimulus of strength a, $\hat{a}$ is the threshold at the 82%-correct point, and E is the Weibull exponent. For detecting a chromatic grating of vector angle 135–315 deg, the threshold $\hat{a}$ for observer C. F. S. was 0·0024 (cone-contrast vector length, VL) and the exponent E was 2·2; for identifying its direction, $\hat{a} = 0{\cdot}0049$ and $E = 4{\cdot}7$. Thus the grating can be detected with high probability (by RG) before a significant motion response is generated (by SPO). Cole *et al.* (1990) also obtained an exponent of ~2 for detection of a chromatic flash. The exponent for motion of this chromatic pattern is considerably higher than for detection. In contrast, for luminance gratings, detection and direction thresholds were equivalent and both exponents were high (>4). Lee & Stromeyer (1989) report similarly high exponents for direction identification, even for motion signalled by S cones. The higher exponent for

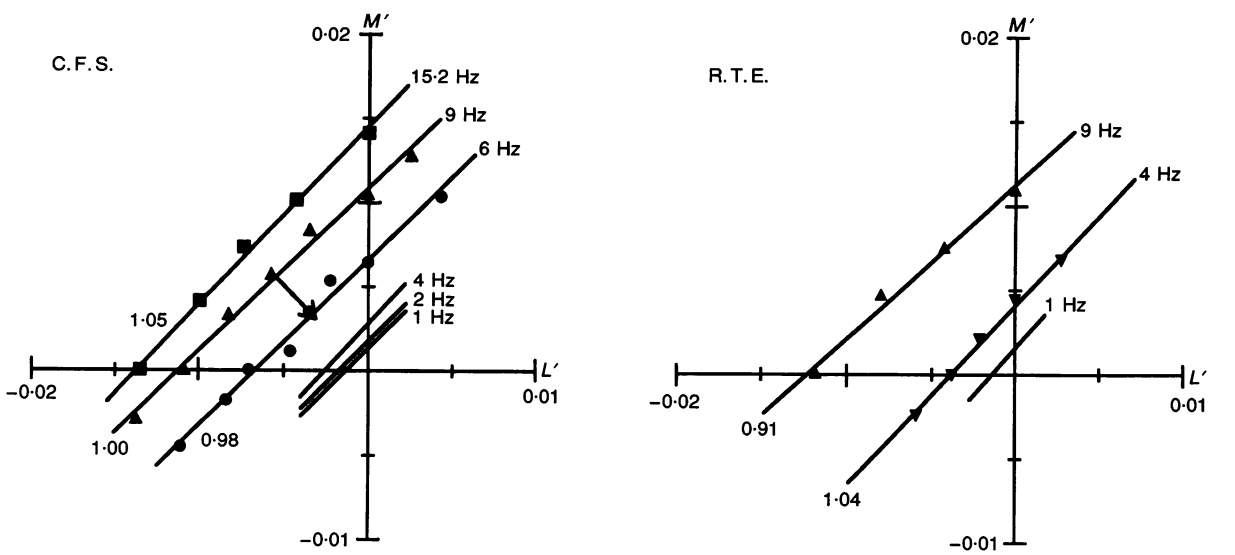

Figure 8. Detection contours for the RG hue mechanism measured with drifting gratings of 1–15 Hz

Contours without data points represent forced-choice detection thresholds (replotted from Figs 2, 3 and 4); other data were obtained with an adjustment procedure (the arrowtip depicts a forced-choice threshold at 9 Hz). Data at 15 Hz are scaled down threefold. The contours have slope of ~1·0, indicating that the L and M contrasts contribute with equal magnitude but with opposite sign, to RG.

the detection of motion than colour suggests that different mechanisms detect these two stimulus attributes.

Our results show that at 4 Hz, the chromatic grating can be detected at twofold lower contrast than that required for seeing motion. We did not make forced-choice comparisons of detection *versus* direction identification at higher temporal frequencies. However, Gegenfurtner & Hawken (1995) recently observed that the direction of motion of foveal, red–green chromatic gratings could be identified at detection thresholds above about 8 Hz. Lee & Stromeyer (1989) observed a similar temporal frequency dependence for moving S cone gratings: at low velocities the pattern could be detected well below the direction threshold, but not so at higher velocities.

Quadrature protocol: separation of the two motion mechanisms

The remaining measurements were obtained with the quadrature protocol and a related flicker protocol, which allow better isolation of the motion mechanisms. Results obtained at 1 Hz will provide an introduction to the quadrature protocol. We will then present an analysis of the protocol and further data.

A brief review of the work of Cavanagh, MacLeod & Anstis (1987), who used the quadrature protocol to make equiluminant settings, will clarify our experiments. They presented a counterphase flickering yellow–dark, luminance grating (a 'pedestal') on a yellow adapting field. A flickering red–green chromatic grating (a 'test') was added to the pedestal with a phase shift of 90 deg in space and time (in spatial–temporal quadrature). Only if the latter coloured grating contained some luminance contrast was motion seen: for example, if the brighter bars of the coloured grating appeared 1/4 cycle to the right of the bright bars of the luminance grating at a point 1/4 cycle later in time, then net motion was seen to the right, because the *luminance* component shifts rightwards over time. If the pedestal and test stimulate mutually independent mechanisms, then each mechanism will signal a standing-wave pattern and no motion will be seen. To generate motion, both components must stimulate a common mechanism.

Separation of LUM and SPO motion mechanisms at 1 Hz

The results for 1 Hz moving gratings (Fig. 2) indicated that the LUM motion mechanism was less sensitive than the SPO mechanism. The quadrature protocol will first be used to measure the detection contour of this less sensitive LUM mechanism, and then the contour of the SPO mechanism.

To isolate LUM, a counterphase flickering pedestal that stimulates only LUM was selected: the pedestal vector angle in (L', M') space was set *parallel* to the SPO contour obtained at 1 Hz (Fig. 2, observer C.F.S.), thereby not stimulating SPO. (Since the stimulus vector is parallel to the SPO detection contour, the vector does not cross the detection contour, thus producing little or no stimulation of the SPO mechanism.) The pedestal, of 46 deg and VL of 0·042, stimulated LUM at ~3 times threshold (Fig. 9, long-dashed vector). We added to the constant luminance pedestal various quadrature tests, covering a range of angles in (L', M') space. The motion of each test pattern was reversed (for forced-choice measurements) by inverting the temporal phase of the test. At each test angle, we measured the test contrast for identifying the direction of motion produced by the combined pedestal-plus-test pattern. Motion can only be seen to the extent that the tests also stimulated LUM. Figure 9 (○) plots the test contrast thresholds *per se*, plotted relative to the origin. The quadrature detection contour (long-dashed lines) is

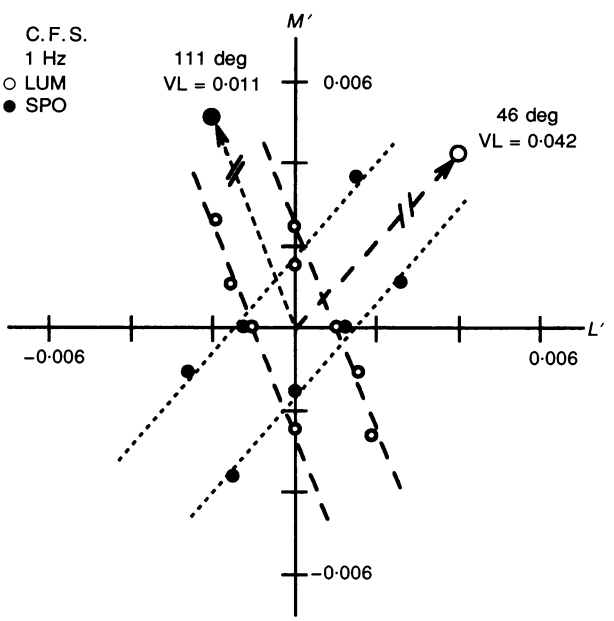

Figure 9. Direction identification thresholds for LUM and SPO measured with quadrature protocol at 1 Hz

The counterphase pedestal was aligned in (L', M') space either to stimulate only LUM (long-dashed vector, *parallel* to SPO contour in Fig. 2) or to stimulate only SPO (short-dashed vector, *parallel* to LUM contour in this figure – long dashes). Near the vector tip we specify both the cone-contrast pedestal angle and vector length, VL. In order to probe the sensitivity of the mechanism isolated by the pedestal, we add to each pedestal a counterphase test in spatial–temporal quadrature phase. The test assumes different angles in the (L', M') space and, at each angle, test contrast is varied to measure direction thresholds for the combined pedestal-plus-test. Thresholds shown here indicate the test contrasts *per se* (plotted relative to origin). The slopes of the fitted lines are also shown in Fig. 2.

relatively steep, with a slope of −2·6, indicating that at 1 Hz the L cones contribute with about 3 times the weight of the M cones to LUM. At high velocities, the L and M cones contribute more equally.

Having measured the quadrature contour for LUM, we then measured the related contour for SPO. The pedestal (Fig. 9, short-dashed vector) was set parallel to the luminance contour, just measured, so that only SPO is stimulated; we used a pedestal of 111 deg and VL of 0·011. The short-dashed lines show the quadrature contour for SPO. The SPO mechanism has very similar slopes whether measured with simple moving gratings (Fig. 2) or with the quadrature protocol (Fig. 9).

Analysis of quadrature protocol

To determine the relative L and M weights of a motion mechanism, we measured detection contours for either simple moving gratings or for flickering gratings in the quadrature protocol. A detection mechanism that linearly combines L' and M' signals will produce a bowed detection contour (a segment of an ellipse) for the simple moving gratings if there is a temporal phase shift between the L' and M' signals within the mechanism. (Measurements presented later demonstrate a substantial phase shift between the L' and M' signals in LUM.) Yet, as the present analysis will show, the contour measured with the quadrature protocol is expected to be *straight* regardless of the phase shift; furthermore, the phase shift will cause the contour slope to depend on the pedestal angle in (L', M') space.

In the quadrature protocol, there are two counterphase patterns (pedestal and test), each composed of equivalent left- and right-moving patterns, and each of these moving patterns gives rise to an L and an M cone motion signal (i.e. an L and an M cone moving grating signal). Phasors allow us to represent the amplitude and phase of these motion signals and predict whether the net motion within a single mechanism will be leftward or rightward.

The phasors in Fig. 10 represent the amplitude and temporal phase of the L and M motion signals within a single mechanism (in this case LUM) referenced to a *single fixed retinal point*. According to convention, phasors rotate one revolution each temporal cycle, with an anti-clockwise rotation indicating a phase advance, and clockwise rotation a phase delay. In the present example, we consider the motion produced by a pure luminance pedestal and a chromatic test pattern that contains a weak luminance component, similar to the experiment of Cavanagh *et al.* (1987) described above.

Each counterphase flickering pattern had balanced left- and right-moving components, so motion could only be perceived by an interaction of the signals from the pedestal and test. Figure 10*A* first depicts the hypothetical signals generated by *one* of the two oppositely moving components of the luminance *pedestal*. The L'_p and M'_p pedestal signals have positive coefficients a and b, representing the L and M cone weights for the LUM mechanism. The M'_p component is arbitrarily drawn with phase referenced to vertical. In this example, the L'_p signal is shown physiologically lagging the M'_p signal by

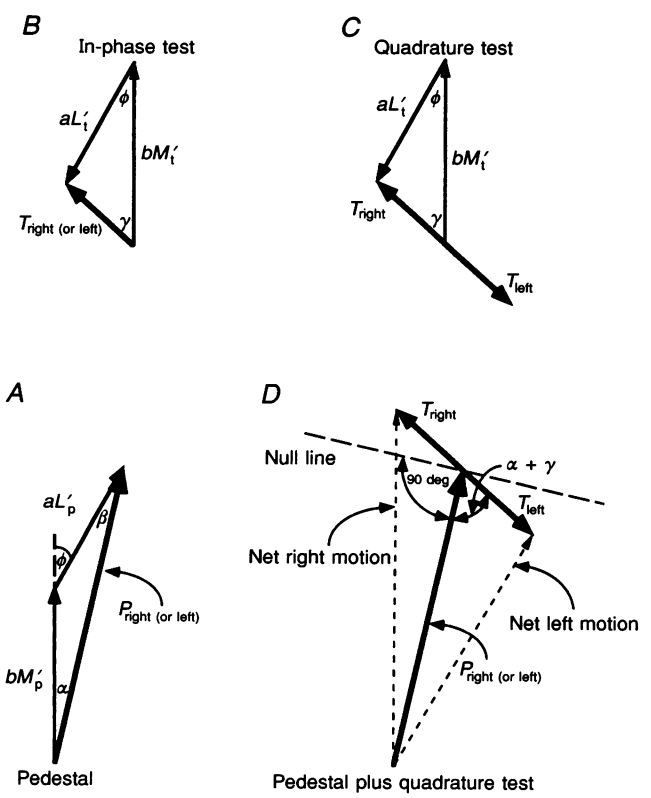

Figure 10. Phasor analysis of quadrature protocol showing that, when there is an intrinsic, physiological phase shift between L' and M' signals within a motion mechanism, the *test* spectral composition (red–green) producing a motion null depends upon the *pedestal* spectral composition (details in text)

A, counterphase pedestal for LUM, with L' signal physiologically lagging M' by ϕ. *B*, counterphase test of different spectral composition from pedestal, shown here first in phase spatially and temporally with pedestal. *C*, same test now shifted 90 deg spatially in phase to right of pedestal and temporally delayed 90 deg. *D*, quadrature test in *C* added to pedestal in *A*. Net motion is rightward, indicted by the longer (dashed) right-motion phasor. An appropriate change of test spectral composition (red–green) will bring left and right test phasors onto the *null* line where left and right motions are balanced. The null line is always orthogonal to the pedestal phasor; hence (when there is an intrinsic phase shift between L and M signals), changing the pedestal spectral composition will change the test spectral composition yielding the null.

temporal phase ϕ. The angle α is determined by the relative magnitudes of signals, L'_p and M'_p, and by the intrinsic phase shift ϕ. The sum phasor (thick arrow, Fig. 10*A*) represents the combined effects of the L'_p and M'_p signals. Because the flickering pedestal has equal left- and right-motions, there are two similar sum phasors P_{right} and P_{left}.

Figure 10*B* and *C* (top) represents the signals generated by the *test* pattern. We first depict (Fig. 10*B*) the effects of the test stimulus physically flickering spatially and temporally *in phase* with the pedestal, *before the quadrature spatial and temporal shifts are imposed*, and thus the L and M test phasors are parallel with the L and M *pedestal* phasors. The test pattern is a chromatic grating with weak luminance contrast; the test has a different red–green spectral composition from the luminance pedestal; thus the L'_t component of the test is negative with respect to the L'_p component of the pedestal. The angle γ is determined by the relative magnitudes of the signals L'_t and M'_t, and by the intrinsic phase ϕ. We next (Fig. 10*C*) impose the quadrature shifts on the test: the flickering test stimulus is shifted 90 deg rightward in spatial phase relative to the pedestal, and temporally delayed by 90 deg. The important feature in understanding this analysis is that the 90 deg rightward spatial shift *advances* the right-moving test component (T_{right}) by 90 deg, but *delays* the left-moving test component by 90 deg, whereas the 90 deg temporal delay, *delays both* left- and right-moving components. For the right-moving component the spatial and temporal phase shifts thus cancel, and consequently, the quadrature shifts produce no change in the right-moving component, but cause a 180 deg phase shift (equivalent to sign inversion) in the left-moving component. The sum phasor in Fig. 10*C* represents the right test signal after (as well as before) the quadrature shifts; the inverse of this sum phasor represents the left test signal.

Finally, the sum phasors for both test and pedestal are added together (Fig. 10*D*) to give the resultant left and right signals. In this example, the net motion is unbalanced, with the right motion stronger (longer dashed phasor). When the phase differential between test and pedestal ($\alpha + \gamma$) equals 90 deg, left and right motion is balanced, and no motion is seen. This null condition is achieved by simply adjusting the amplitude ratio of the L' and M' test components (the red–green test mixture) to bring the test phasors onto the 'null line' that is orthogonal with the pedestal (Fig. 10*D*), so that the dashed phasors for net left and right motion are of equivalent length.

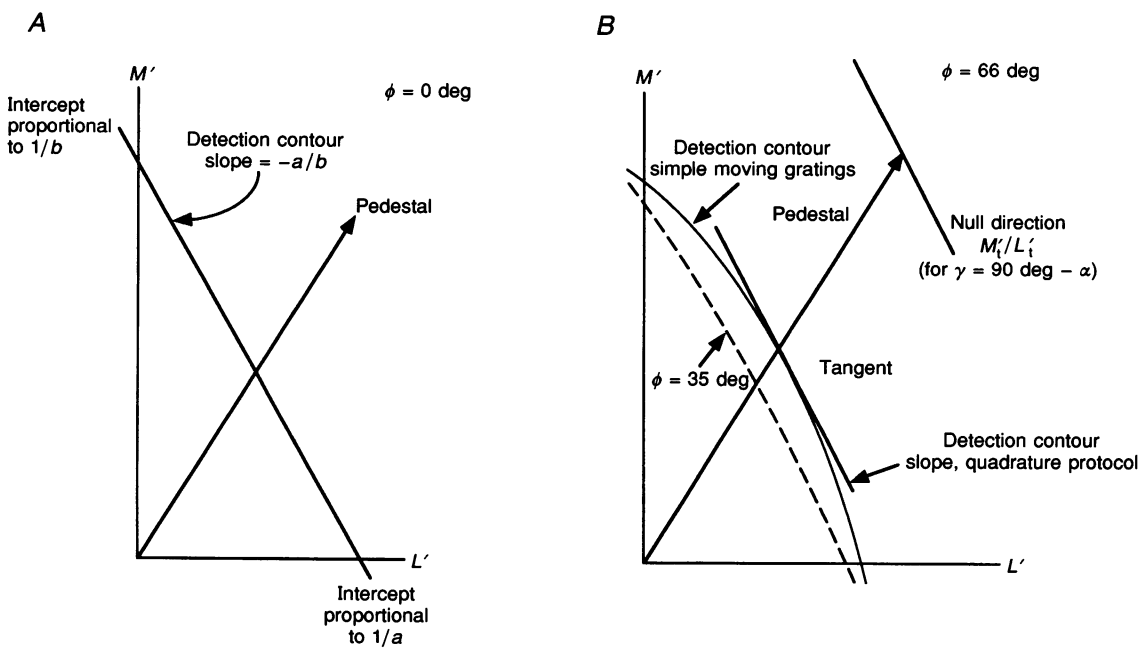

Figure 11. Effect of intrinsic phase shift on detection contours for simple moving gratings *versus* quadrature protocol

A, with no intrinsic, physiological phase shift between the L' and M' signals ($\phi = 0$ deg), the LUM contour is straight when measured with simple moving gratings. *B*, an intrinsic phase shift (e.g. $\phi = 66$ deg) produces a curved detection contour (continuous elliptical arc) for the simple gratings, but the contour for the quadrature protocol remains straight – its slope is tangent to the ellipse where the quadrature pedestal intersects the arc. The slope of the quadrature contour specifies the test spectral composition yielding the motion null. The dashed line shows that the detection contour for simple moving gratings is reasonably straight for a fairly large phase shift, $\phi = 35$ deg.

We measured detection contours with the quadrature protocol using a range of test stimuli having different angles in (L', M') space (e.g. Fig. 9). The contour represents a criterion (just-visible, threshold-level) imbalance between the left and right motions for each test stimulus. Thus the detection contour must be approximately straight and parallel to the null line (providing the pedestal strength is at least about thrice the test strength, in order that small angle approximations remain valid). If there is an intrinsic physiological *phase* lag between the L and M signals, the orientation of the null line will depend on the relative magnitude of the L' and M' pedestal signals (as shown in Fig. 10*D*). In this case, a change of the pedestal angle in (L', M') space will change the red–green test mixture producing the motion null, and consequently change the orientation of the detection contour.

If there is no intrinsic phase shift between the L' and M' signals, then both γ and α (Fig. 10) are zero, and left and right motion is balanced when the L' and M' test phasors sum to zero in the luminance mechanism,

$$aL'_t + bM'_t = 0, \text{ hence } \frac{M'_t}{L'_t} = -\frac{a}{b}.$$

In this case (Fig. 11*A*), the detection contour for the simple moving gratings will be straight, with the slope matching the slope obtained with the quadrature protocol; the quadrature slope is equal to the ratio of the cone weights, $-a/b$. When there is an intrinsic phase shift between the L' and M' signals (Fig. 11*B*), the detection contour for the simple moving gratings is an elliptical arc. The continuous line shows that there is considerable bowing for a large phase shift such as $\phi = 66$ deg. Significant bowing only occurs for a phase shift greater than ~45 deg (Stromeyer *et al.* 1987). The dashed line, for example, shows that the contour for simple moving gratings is relatively straight when ϕ is 35 deg. As demonstrated in the next paragraph, the slope measured with the quadrature protocol is tangent to the elliptical contour (Fig. 11*B*) at the point where the pedestal vector intersects the arc. For phase shifts below about 30 deg, the contour for simple moving gratings will be quite straight, and thus the tangent quadrature slope ought to give reasonably good estimates of the cone weights of the isolated motion mechanism.

Consider a simple moving LUM grating with components aL' and bM' (as in Fig. 10*A*). The grating is detected at a criterion, called D, representing a fixed magnitude of the sum phasor. Trigonometry yields:

$$aL'\cos(\phi - \alpha) + bM'\cos\alpha = D,$$

subject to the constraint

$$aL'\sin(\phi - \alpha) = bM'\sin\alpha.$$

We take the total differential of the first of these with respect to all three variables (L', M' and α)

$$\mathrm{d}D = 0 = a\mathrm{d}L'\cos(\phi - \alpha) + b\mathrm{d}M'\cos\alpha + \mathrm{d}\alpha[aL'\sin(\phi - \alpha) - bM'\sin\alpha],$$

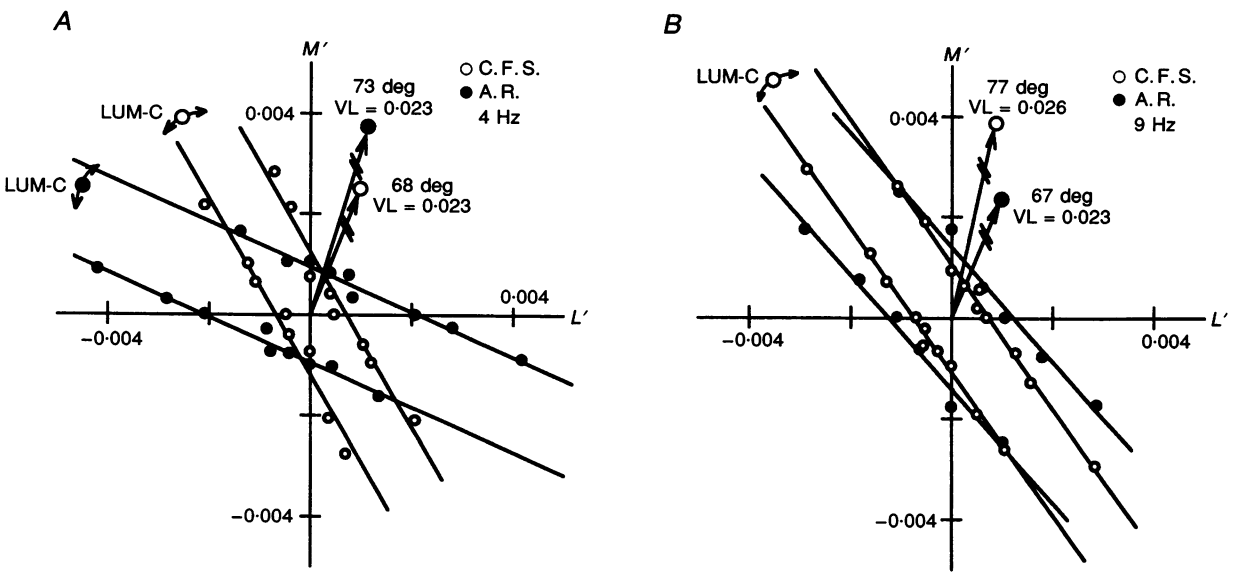

Figure 12. Quadrature contours for LUM mechanism at 4 and 9 Hz

Vectors specify the pedestal angle and vector length, VL. LUM-C (luminance cross-overs) show where the motion reverses, or crosses over, measured with higher contrast tests (VL, 0·015–0·02). The small arrows indicate that the test vector was rotated to different positions in the cone-contrast space to find the cross-overs.

then we apply the constraint, which eliminates the variation $d\alpha$. This gives

$$-\frac{dM'}{dL'} = \frac{a\cos(\phi - \alpha)}{b\cos\alpha},$$

which represents the tangent to the detection contour (ellipse) in the L', M' diagram. Figure 10*A* shows that the value of α depends on the ratio M'/L' and so the tangent slope is related to each specific value of M'/L' (the parameters a, b and ϕ reflect the invariant properties of the detection mechanism).

From Fig. 10*B* we can write the relation involving the phase angle γ of the test signal in the quadrature protocol

$$-\frac{bM'_t}{aL'_t} = \frac{\sin(\gamma + \phi)}{\sin\gamma},$$

since $a < 0$, as depicted in Fig. 10*B*.

The null condition in the quadrature protocol, $\alpha + \gamma = 90$ deg, leads to

$$-\frac{M'_t}{L'_t} = \frac{a\cos(\phi - \alpha)}{b\cos\alpha},$$

which is identical to the differential above. Thus the quadrature detection contour has a straight slope, tangent to the detection ellipse for the simple moving gratings.

Luminance motion contours measured with quadrature protocol

Our analysis indicates that the contours for the quadrature protocol must be straight. Straight contours were observed at 1 Hz (Fig. 9) and are confirmed at 4 and 9 Hz for the LUM motion mechanism (Fig. 12). Sensitivity on the pedestal is often extremely high: the test can produce visible motion at as low as 0·05% contrast (Stromeyer *et al.* 1984). Additional data obtained at 2, 6 and 17·7 Hz (not shown) were also well fitted by straight lines (correlation coefficients, r^2, 0·96–1·00). For these measurements, the pedestal angle was set approximately parallel to the slope of the contour of the SPO mechanism measured with the simple moving gratings. The slopes of the contours obtained with the quadrature protocol were compared with the detection contours for simple moving gratings in Figs 2–6; the pedestal angles are depicted by the dashed vectors. As predicted, these quadrature contours (dashed lines) have slopes approximately tangent to the detection contours for the simple moving gratings at the point where the pedestal vector intersects the latter contours.

Cavanagh *et al.* (1987) used high-contrast patterns with the quadrature protocol to make equiluminant settings, defined as the test spectral composition yielding a motion null. The pedestal was a luminance grating; the test vector was rotated to different angles in the (L', M') space to find the point at which the motion reverses direction, or 'crosses over'. We measured psychometric functions for left–right direction judgements as a function of test vector angle. The cross-over is given by the 50% point on the psychometric function; the motion reverses to either side of this point. At the cross-over the motion is nulled, and thus the cross-over ought to be parallel to the quadrature detection contour. We measured cross-overs at 4 and 9 Hz, designated LUM-C (luminance cross-over) in Fig. 12, using a moderate contrast test (VL ≈ 0·02); the pedestal was the same as for the quadrature contours. As shown, the cross-overs are approximately parallel to the quadrature contours. The slight difference may have been caused by the measurements being made on different days.

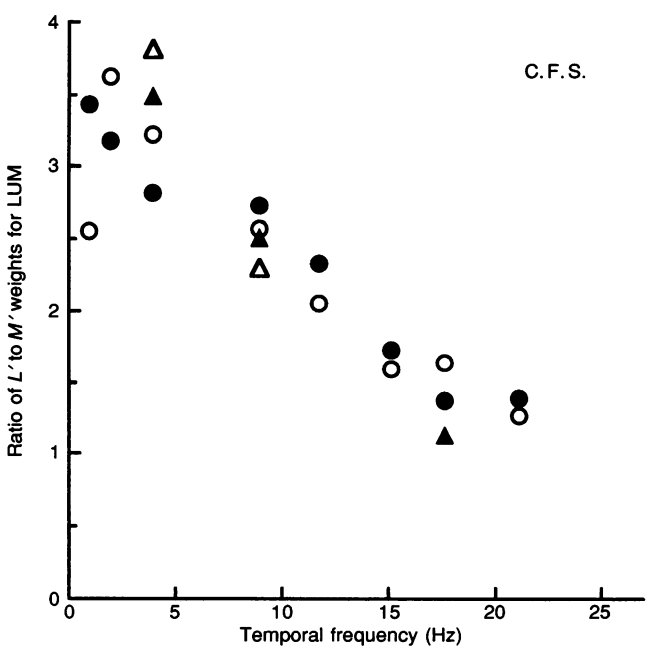

Figure 13. Ratio of L' to M' weights for LUM as a function of temporal frequency

The pedestal was 45 deg in (L', M'). The weights were assessed with both motion and flicker: for motion, the estimates are from slopes of quadrature motion contours (○) and motion cross-overs (●); for flicker, from slopes of flicker contours (△) and flicker cross-overs (▲).

The quadrature contours for observers C. F. S. and R. T. E. indicate that the LUM mechanism is dominated by the L' signal at low velocities. To show this more clearly, the quadrature contours and motion cross-overs were remeasured for C. F. S. from 1 to 21 Hz, using a pedestal of vector angle 45 deg and ~2 times threshold. Figure 13 shows that the L' signal is about 3 times more effective than the M' signal at low velocities; at the high velocities, the two signals are more comparable.

Luminance flicker: comparison with luminance motion

The previous results were based on motion judgements. The luminance mechanism is traditionally studied with flicker rather than with motion. We can readily modify the quadrature protocol to assess whether the relative L' and M' weights are similar for both luminance motion and flicker. The contours and cross-overs were remeasured, using a flicker discrimination protocol in which there is no motion imbalance (Lee & Stromeyer, 1989). The flicker cross-over represents the vector angle in (L', M') space at which the test flicker reverses luminance polarity, analogous to the motion cross-over. The counterphase flickering pedestal and test (1 cycle deg^{-1}) were presented *spatially in phase* (not in quadrature spatial phase). The pedestal, set near threshold at 45 deg in (L', M') space, was presented in both temporal intervals of a trial. The test was presented at the *same* contrast in both intervals: in one interval it was added in phase temporally with the pedestal, and in the other interval it was simply inverted in temporal phase. This stimulus produces no motion imbalance; the observer judges which interval contains the stronger luminance flicker ('agitation').

Measuring the flicker cross-over provides a far more sensitive way of assessing minimal luminance than the conventional method of heterochromatic flicker photometry, wherein the radiance of red flickering light is adjusted relative to antiphase green light to minimize subjective luminance flicker. Recall that to find the flicker cross-over, we vary the angle of the test stimulus in (L', M') space. To one side of our cross-over the green test luminance is greater than the red, and to the other side, the red luminance is greater than the green. This weak residual luminance flicker is perceptually magnified by our procedure of adding near-threshold yellow flicker (the

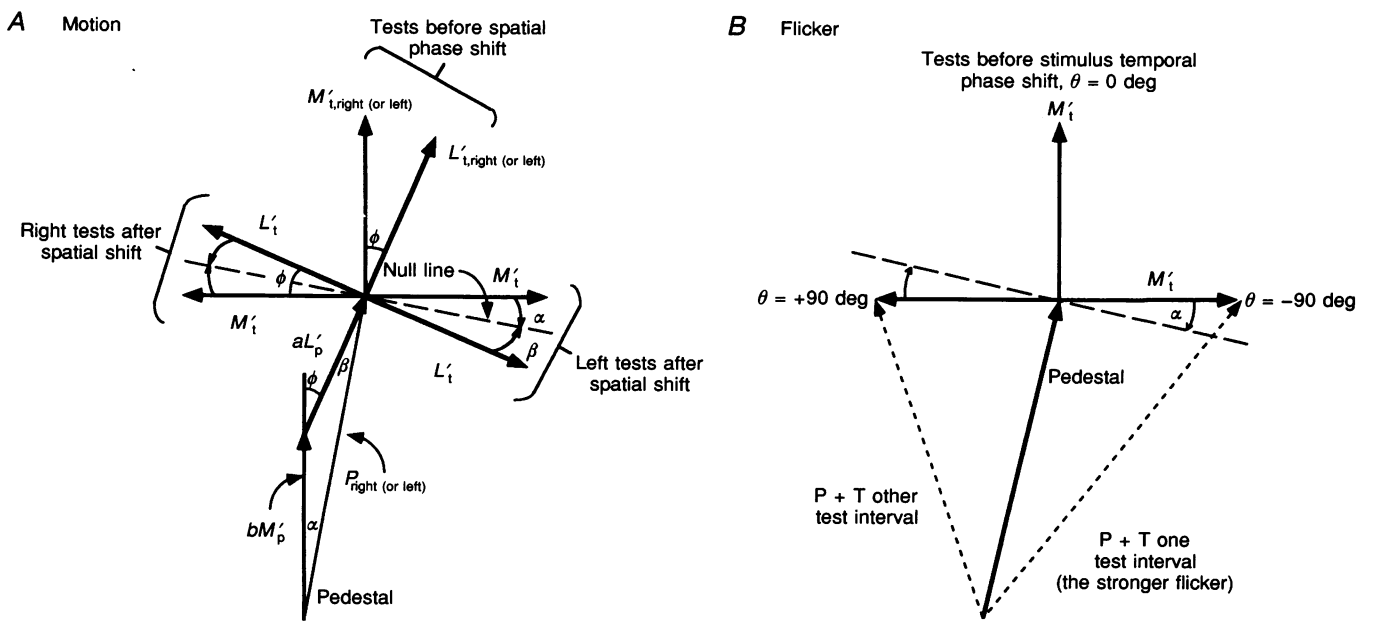

Figure 14. Phasor representation for measuring the intrinsic physiological phase shifts, ϕ, between L' and M' signals within LUM (details in text)

The pedestal is similar to that depicted in Fig. 10*A*, with the L' signal lagging M'. The dashed line is the null line. *A*, quadrature protocol with motion criterion: L and M test stimuli are used separately. Each is presented in quadrature spatial phase with pedestal and is adjusted in temporal phase to lie on the (motion) null line. The sum of required phase shifts for the null, measured with the separate L test and M test, specifies the intrinsic phase shift, $|\phi| = |\alpha| + |\beta|$, as shown here by geometrical construction. *B*, analogous flicker discrimination protocol. The test stimulus is presented spatially in phase with pedestal and is temporally inverted between the two test intervals (θ *versus* $\theta - 180$ deg). Shown here is the M test, which must be adjusted in temporal phase in order to lie on the (flicker) null line, where the effective flicker of test-plus-pedestal is equivalent in the two temporal intervals, thus making the discrimination impossible. Again the intrinsic phase lag, $|\phi|$, is equivalent to the sum of $|\alpha|$ and $|\beta|$ for the M and L tests, respectively.

pedestal) in *opposite* temporal phases with respect to the test in the two trial intervals. In one interval, the pedestal and test effectively summate, whereas they cancel in the other interval. The two trial intervals occurring close in time, allow a simple relative judgement of flicker strength. The pedestal is without effect when the red and green test flickers are matched at the equiluminant cross-over, as defined by the 50% (chance) point on the psychometric function.

The relative L' and M' weights are similar for the flicker (Fig. 13) and motion judgements, suggesting that a common mechanism underlies both judgements. This is supported by phase measurements, presented next.

Temporal phase of L *versus* M signals in the various mechanisms

To measure the relative temporal phase of L and M signals within the two motion mechanisms and RG hue mechanism, we used variations of the quadrature protocol and the flicker discrimination protocol (Lee & Stromeyer, 1989; Stromeyer, Eskew, Kronauer & Spillmann, 1991*a*). Information about phase is important in specifying how the L and M signals combine in each mechanism, and differences in phase between mechanisms may allow us to further differentiate the mechanisms.

Phase shifts within the luminance motion mechanism

If there was only a single motion mechanism, we could measure the L *versus* M phase shift with an L cone pedestal and an M cone test. However, there are two motion mechanisms, and we wanted the motion judgements to be mediated by only one of these. As before, we set the pedestal to a vector angle in (L', M') space to stimulate effectively one motion mechanism, while producing little or no stimulation in the other mechanism. We then used separate L and M cone tests to assess relative phase.

Figure 14*A* shows how a simple variation of the quadrature protocol can be used to measure the relative phase of the L' and M' signals in the LUM motion mechanism, using the separate L and M cone tests. The pedestal is similar to that depicted earlier (Fig. 10*A*), where the L'_p signal is shown with an intrinsic, physiological phase lag ϕ relative to M'_p. We wished to measure lag ϕ between the L' and M' signals in LUM. To do this we used an L and an M test separately. We have shown phasors for *both* tests in Fig. 14*A*, so that the reader can see by geometrical construction that $|\phi|$ is equal to the sum of the phase shifts, $|\alpha|$ and $|\beta|$, measured with the two separate tests. We now consider the phasors for each test.

First, let us consider just the M cone test. The vertical phasor M'_t first depicts the M cone test stimulus physically flickering *in phase* spatially and temporally with the counterphase pedestal stimulus. In the actual experiment the test is shifted rightward 90 deg in spatial phase relative to the pedestal, which causes the M'_t left- and right-motion phasors to shift 90 deg in opposite directions as shown. This will produce a motion imbalance (as explained Fig. 10), but this can be eliminated by next shifting (i.e. *delaying*) the *temporal* phase of the M cone test by α deg, placing the M'_t phasors on the null line where motion is balanced. Analogous phasors are shown for the L cone test: the L'_t phasor tilted slightly right of vertical, first depicts the stimulus physically flickering in phase with the pedestal stimulus; after this counterphase test is shifted 90 deg rightward in spatial phase, it must be *advanced* in temporal phase by β deg to place the phasors on the null line. It should be clear from our construction (Fig. 14*A*) that the physiological phase shift, ϕ, is equal to $\alpha + \beta$ (the difference between the advanced

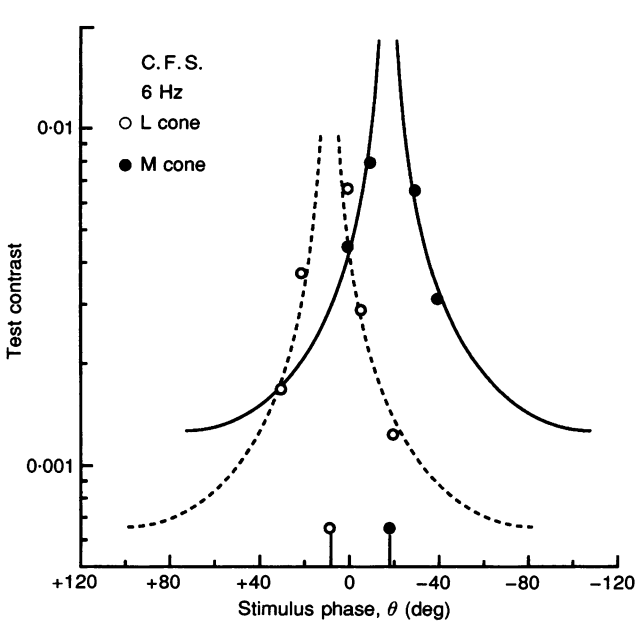

Figure 15. Measurement of intrinsic L' and M' phase shifts in LUM at 6 Hz, using quadrature protocol

The contrast of direction thresholds is shown here for the separate L and M tests as a function of stimulus *temporal* phase, θ, relative to that of a luminance pedestal of 45 deg in (L', M'). The intrinsic phase shift, ϕ, between the L' and M' signals is specified by the difference between the vertical symmetry axes of the two templates: the L' signal lags M' by 26 deg. (The abscissa represents time advancing rightward, and thus a stimulus phase advance (i.e. earlier time) is plotted with positive values toward the left. This latter convention is opposite to that used in Lee & Stromeyer (1989).)

phase shift required for the L test and the delayed shift for the M test). The required temporal phase shifts, α and β can also be used to estimate the relative weights of L' and M' in the luminance mechanism since,

$$\frac{aL'_p}{bM'_p} = \frac{\sin|\alpha|}{\sin|\beta|}.$$

To measure the temporal phase that produces the motion null, we used a template fitting procedure, described in detail by Lee & Stromeyer (1989). Motion thresholds were measured for a range of temporal phases of the test pattern, θ, relative to the pedestal. In a linear system the magnitudes of these contrast thresholds follow an inverse sine relationship

$$|\sin(\theta - \theta_0)|^{-1},$$

where θ_0 is the temporal phase of the test stimulus that produces the motion null. Figure 15 shows an example of templates for the separate L and M test stimuli, measured at 6 Hz. The pedestal was set to 45 deg in (L', M') space at ~2 times threshold. Each point represents the test contrast threshold for discriminating left *versus* right motion, produced by presenting the test stimulus at temporal phase θ *versus* $\theta - 180$ deg (inverted temporal phase); θ is depicted on the horizontal axis in Fig. 15. The phase difference between the L and M cone templates was 26 deg, indicating a 26 deg lag of the L' signal relative to M'. The phases at the horizontal asymptotes of the templates (90 deg away from the peaks) are the phases of optimal L' and M' combination; thus the ordinate values of these asymptotes also give the relative L' and M' weights in the LUM mechanism.

Similar pairs of templates were measured for observer C.F.S. at 1–21·2 Hz, and the phase lags were extracted. For C.F.S. (Fig. 16, ○), the L' signal lagged M' except at the highest velocity, where the phase weakly reversed. The phase shifts are surprisingly large at intermediate frequencies: more than 30 deg at 9 Hz. Comparable phase shifts (●) were obtained for observer A.C., using an abbreviated procedure where we identified the stimulus phase at the template peaks, by measuring psychometric functions for direction discrimination as a function of temporal phase, for the separate L and M tests; the discrimination is worst at the phase corresponding to the template peaks. The somewhat larger phase shifts for A.C. may be caused by the slightly longer wavelength of the field used, 580 nm *versus* 577 nm for C.F.S. (see Discussion).

Phase shifts within the luminance flicker mechanism

Limited phase measurements were also made with the flicker discrimination protocol, in which the counterphase pedestal and test are presented *spatially* in phase. This protocol is illustrated in Fig. 14*B*, where the pedestal is equivalent to that depicted for the motion protocol (Fig. 14*A*). In one interval of a trial, the flickering test is presented at temporal phase θ with respect to the pedestal and in the other interval it is presented at the *same contrast* with inverted temporal phase, $\theta - 180$ deg. If there were no intrinsic phase shifts between the L' and M' signals, then flicker discrimination would break down when test flicker was added to the pedestal in opposite temporal quadrature phases in the two intervals (at $\theta = +90$ deg *versus* $\theta = -90$ deg), since quadrature temporal phases would equate the strength of the luminance flicker of the pedestal-plus-test in the two intervals. Figure 14*B* shows that if there is a phase difference between the L' and M' cone signals, then adding the test stimulus (in this case M'_t) in temporal

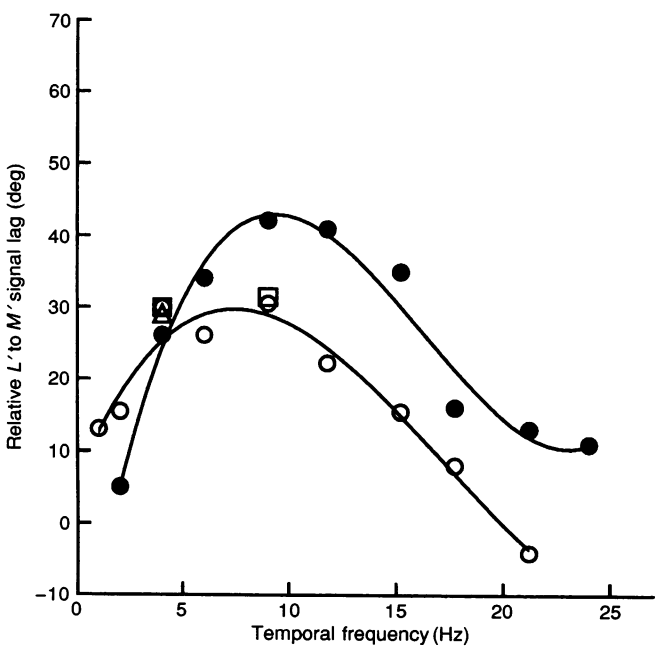

Figure 16. Intrinsic phase shift between L' and M' signals in LUM as a function of temporal frequency, assessed with quadrature protocol

For observer C.F.S. the pedestal was set to 45 deg in (L', M') (○) or, to isolate LUM better it was set to 67 deg at 4 Hz and 71 deg at 9 Hz (□); this made little difference. Phase shifts were obtained for A.C. (●), using a related method. Measurements for C.F.S. were also made with the flicker discrimination protocol (△). Smooth curves simply connect points and have no theoretical import.

quadrature will produce a contrast difference between the test-plus-pedestal for the two trial intervals. The long-dashed phasor shows the test interval with stronger flicker. To eliminate the flicker difference, we must temporally shift (delay) M'_t by α deg to lie on the dashed null line (just as in the motion protocol). The L cone test (not shown) must be temporally advanced by β deg to lie on the null line. The physiological phase shift $|\phi|$ is again simply the sum of the two required phase shifts, $|\alpha| + |\beta|$. The template for flicker has the approximate form

$$|\cos(\theta - \theta_0)|^{-1},$$

where θ_0 is the stimulus phase for zero effective contrast difference between the two trial intervals.

We measured the phase shift for LUM at 4 Hz and 1 cycle deg^{-1}, using a pedestal of vector angle 55 deg and separate L and M tests. The L' signal lagged M' by 29 deg (Fig. 16, △). The fact that the phase shift is so similar for luminance flicker and motion, and the fact that the cone weights are so similar for the two judgements (Fig. 13), suggests that a single mechanism underlies both.

Phase shifts within the red–green hue mechanism

The flicker discrimination protocol was also used (with the 1 cycle deg^{-1} gratings) to measure phase templates for the RG hue mechanism. The task, however, was to choose which interval appeared to have the greater red and green hue, thus probing the RG hue mechanism (Stromeyer *et al.* 1991*a*). We used a pure L cone pedestal, set approximately *at threshold*, and a pure M cone test. At 2 and 4 Hz the task was easy, since colour without luminance flicker was seen at most temporal phases for these very weak stimuli. For observer C.F.S. the L to M phase shift was 0 deg at both frequencies; at 6 and 9 Hz, it was 1 and 2 deg. At 9 Hz the task was more difficult near the template peak owing to the intrusion of luminance flicker. Measurements for observer A.C. showed a phase shift of 1 deg at 6 Hz. Thus any phase shift within RG is small (at 9 Hz and below), and is very different from the large phase shift within LUM.

Phase shifts within the spectrally opponent motion mechanism: an iterative procedure

The quadrature motion protocol was next used to measure the phase shift within SPO. If the SPO and LUM motion mechanisms both exhibit large phase shifts, it would be difficult to choose a pedestal that stimulates only one of the mechanisms. However, the present measurements suggest that the phase shifts are small within SPO. Since LUM appears to exhibit a large phase shift, a high-contrast counterphase grating is likely to stimulate LUM to some extent regardless of its orientation in (L', M') space. To measure the phase shifts in SPO we need a pedestal that is 'silent' for LUM: we used a counterphase pedestal, the L and M components of which were shifted in *temporal* phase relative to each other to compensate for the relative phase shift of the L' and M' signals within LUM.

Consider the iterative steps taken at 4 Hz, for observer C.F.S. From the results in Fig. 16, we initially estimate that L' lags M' by ~30 deg in the LUM mechanism; the horizontal asymptotes of the phase templates (not shown) provide an estimate of the L' and M' weights for LUM. The L and M horizontal asymptotes of 0·00070 and 0·00185, respectively, imply a contour slope for LUM of 111 deg in (L', M') space. To silence LUM and thus only stimulate SPO, we used a counterphase pedestal of 111 deg in (L', M') space, with the L' component of the pedestal temporally advanced by 30 deg relative to the M' component, to compensate for the L lag. The pedestal was set to ~2 times threshold, and L and M cone phase templates were separately measured for SPO. The

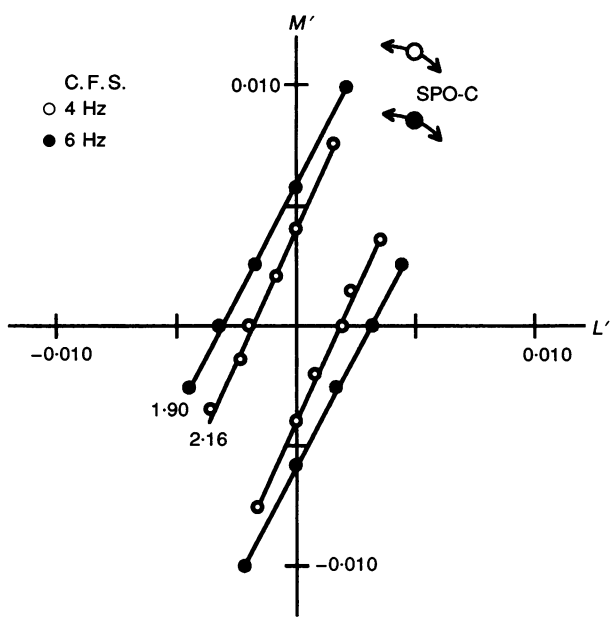

Figure 17. Contours for SPO motion mechanism with quadrature protocol, at 4 and 6 Hz

The counterphase pedestal was intended to stimulate only SPO; LUM was silenced by appropriate adjustments of the amplitude and temporal phase of the L and M components of the pedestal. Also shown are the SPO motion cross-overs, SPO-C. The small arrows indicate rotation of the test vector to find the cross-overs.

separation between the templates indicated that the $-L'$ signal lagged M' by only 2 deg within SPO. In the next iteration, the LUM phase templates were remeasured with a pedestal intended to silence SPO: a pedestal of 55 deg in (L', M') space (determined from the horizontal asymptotes of the SPO templates), with the L and M components approximately in phase. The results indicated that the L' signal lagged M' by 32 deg in LUM. In the last step, the SPO templates were measured a second time with a pedestal of 118 deg with the L component leading by 32 deg. The results indicated that the $-L'$ signal lagged M' by 3 deg in SPO.

The results of this iterative procedure at 4 and 6 Hz show that the L' signal lags M' by a large amount in LUM, ~30 deg, whereas in SPO the lag of $-L'$ with respect to M' is small, 3 and 6 deg, respectively. The fact that the phase shift is small in SPO makes our procedure feasible. Had the phase shift been large in both mechanisms, it would have been difficult to find a pedestal that silences each mechanism in turn.

Spectrally opponent motion detection contours with quadrature protocol

To measure the SPO detection contour we used pedestals that approximately silence LUM. The SPO contour previously measured at a low frequency of 1 Hz (Fig. 9) was obtained with a pedestal which had no phase shift between its L and M components; this may have approximately silenced LUM, since the L *versus* M phase shift is small in LUM at 1 Hz. In the preceding section, we found pedestals that approximately silenced LUM at 4 and 6 Hz, where the phase shifts are considerably larger. These pedestals are now used to measure the detection contours and motion cross-overs for SPO. For the measurements at 4 and 6 Hz, the pedestal vector angle was set to 118 and 112 deg (VL = 0·022), and the L component of the pedestal was temporally advanced in phase by 32 and 31 deg relative to the M component, in order to silence LUM. The test itself was presented at the approximately optimal temporal phase (as determined by the phase templates measured in the previous section). The SPO contours (Fig. 17) show that the L cone weight is about twice the M cone weight – which should be contrasted with the equal weights for the RG hue mechanism (Fig. 8). The motion cross-overs (SPO-C) are approximately parallel to the contours. At the SPO cross-over the test stimulus has strong luminance contrast yet it produces no motion (since the pedestal leaves LUM unstimulated). This is just the converse of the luminance cross-over experiment of Cavanagh *et al.* (1987), in which an equiluminant test produces no motion.

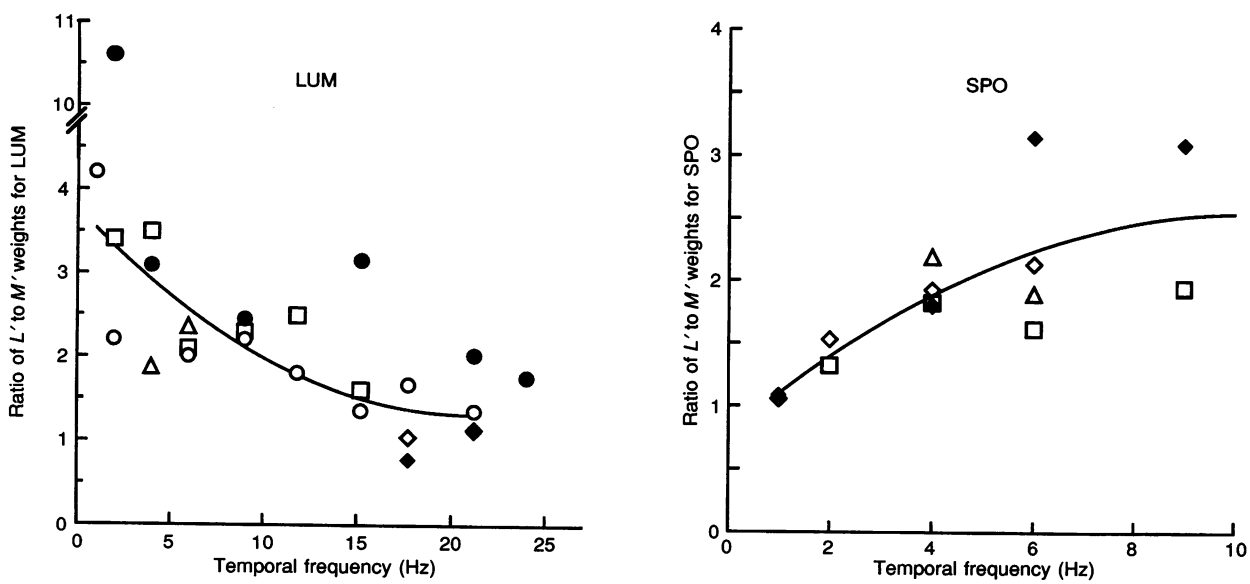

Figure 18. Ratio of L' to M' weights for LUM and SPO motion mechanisms as a function of temporal frequency

Smooth curves are fitted to geometric means of data at each frequency. For LUM, L' has relatively greater weight at low temporal frequencies, and L' and M' are more comparable at high frequencies. An opposite tendency is seen for SPO, where L' dominates at higher frequencies. The weights estimates for LUM are based on various sources: the slopes of the LUM motion contours for simple moving gratings of high velocity (◇, C.F.S; ◆, R.T.E.), the horizontal asymptotes of the L and M LUM phase templates (○, C.F.S.; ●, A.C.) (including templates measured with the iterative procedure, △, C.F.S.), and the separation of the symmetry axis of the phase templates (derived from the equation in the phase analysis, □, C.F.S.). The SPO estimates are based on two sources: the quadrature contours (△, C.F.S.) and, for simple moving gratings, the ratio of direction thresholds along the vertical and horizontal axes of the (L', M') co-ordinates (◇, C.F.S.; ◆, R.T.E.; □, A.R.).

In the analysis of the quadrature protocol (Fig. 10), we concluded that the contour slope will be influenced by an intrinsic, physiological phase shift of the L' and M' signals. If this intrinsic phase shift is zero, the slope will be unaffected by introducing a phase shift between the L and M stimulus components in the *pedestal*, as in the present experiment. The situation of no intrinsic phase shift is special, since a single fixed ratio of the red and green test components produces a motion null regardless of the pedestal phasor angle (Fig. 10). Our phase measurements indicate little phase shift in SPO, and consequently the slope of the quadrature contour directly reflects the L' and M' weights for SPO.

Summary of L and M contrasts weights for the two motion mechanisms

Figure 18 summarizes the L and M contrasts weights for LUM and SPO as a function of temporal frequency. The estimates, from the various experiments, are generally consistent in showing that for three of our four observers L' contributes more than M' to LUM at low temporal frequencies, and the contributions are more similar at high temporal frequencies. Thus a single 'equiluminant' setting is not valid for all temporal frequencies. For the SPO mechanisms, L' and M' contribute about equally at 1 Hz. As temporal frequency increases, the mechanism is more dominated by the L cones. In contrast, the relative L' and M' weights for red–green hue judgements are constant at about 1·0 at all temporal frequencies (Fig. 8).

DISCUSSION

Psychophysical evidence for two motion mechanisms

We initially thought we might well be able to isolate the luminance pathway by measuring motion thresholds if indeed this mechanism was primarily responsible for sensing motion. At low velocity (1 Hz), the direction of motion of the luminance grating could be seen just at detection threshold, whereas chromatic gratings had to be raised ~2 times above detection threshold to see their motion. Even so, at this low velocity the motion sensitivity was a full four times greater for the chromatic gratings than for the luminance grating, thus providing a considerable range below the luminance threshold for measuring the motion detection contour of the coloured gratings. Velocity had to be raised above 9 Hz before we could see an appreciable portion of the luminance contour.

Over the velocity range for which we measured both direction and detection thresholds for chromatic gratings (1–4 Hz), the direction : detection threshold ratio did not much exceed 2 : 1. This is similar to the results of Cavanagh & Anstis (1991), Mullen & Boulton (1992*a*) and Derrington & Henning (1993) for equiluminant gratings, although a larger ratio may be obtained outside the fovea (Lindsey & Teller, 1990; Derrington & Henning, 1993; Palmer, Mobley & Teller, 1993; Gegenfurtner & Hawken, 1995). The detection threshold for our low-velocity chromatic patterns appears to be mediated by the RG hue mechanism, having equal and opposite L' and M' weights, as shown by the detection contours of slope of ~1·0. A slope of ~1·0 was measured for the RG mechanism up to 15 Hz by using an explicit hue criterion for detection. The mechanism signalling the motion of the chromatic gratings appears distinct from this RG mechanism, since the motion contour steepens as velocity is raised, showing a relative attenuation of the M signal. We called this the spectrally opponent motion mechanism, since the contour has a positive slope, indicating a response to the difference of L' and M'. The SPO mechanism could be reasonably well isolated from 1 to 4 Hz by measuring direction thresholds for simple moving gratings, since SPO was the more sensitive mechanism over this velocity range. Steepening of the SPO contour was also seen between 1 and 4 or 6 Hz with the quadrature protocol.

Several lines of evidence suggest LUM and SPO are distinct. There is a clear difference in the shape of the motion detection contours for simple drifting gratings at different velocities. At low velocity, SPO is dominant and LUM has low sensitivity; at high velocity, these roles are reversed; and at intermediate velocities both mechanisms appear to have similar sensitivities and thus cannot be clearly differentiated by measurements using simple moving gratings. At an intermediate velocity of 6 Hz (Fig. 5), for example, the thresholds can be reasonably fitted by an ellipse, which does not allow us to separate individual mechanisms. At lower velocities the SPO mechanism had higher sensitivity and we could align the pedestal in the quadrature protocol parallel to the SPO contour in order to probe the sensitivity of LUM. At high velocities, the direction contours for simple moving gratings are often distinctly non-elliptical, and the LUM contour is fairly well represented.

We also showed that the LUM and SPO mechanisms were distinct by measuring the L' *versus* M' phase shifts in each mechanism. LUM manifests a large relative L' lag at intermediate velocities, where SPO shows little shift. These phase shifts do not reflect the temporal properties of the L and M cones *per se*, for the phase shifts are different within the various post-receptoral mechanisms. RG and SPO manifested little phase shift, whereas LUM showed shifts of 30 deg and more at 4–9 Hz. Lindsey, Pokorny & Smith (1986) and Swanson, Pokorny & Smith (1988) have observed related LUM phase shifts in detecting a pair of red and green flickering lights presented with different relative temporal phases. On an orange field, the luminance flicker mechanism was isolated above 4 Hz. At intermediate temporal frequencies, the red light had to lead green for best sensitivity, indicating that the L signal effectively lagged M; at higher temporal frequencies (> 16 Hz) the phase weakly reversed (Swanson *et al.* 1988). Lindsey & Teller (1988) measured a related LUM

phase shift with moving gratings of 0·5 cycle deg^{-1} and 4–15 Hz. Our method allowed us to isolate each mechanism in turn, and measure the phase shift between the functional L and M signals within each mechanism over a broad frequency range (e.g. 1–21 Hz for LUM and 2–9 Hz for RG).

A large LUM phase shift has implications for the motion quadrature protocol of Cavanagh *et al.* (1987), which is used to set equiluminance. If there is an L *versus* M phase shift, then the null point (the motion cross-over) will depend on the pedestal angle in (L', M') space and the null will not reflect a true equiluminant point. This is vividly illustrated by the following observation: we measured the motion cross-over at 9 Hz (with a luminance pedestal), and then flickered the *same* test grating temporally *in phase* with the pedestal and saw clear motion (pedestal and test were maintained in quadrature spatial phase). Clearly the test pattern is not equiluminant since it produces luminance motion; for equiluminance, one must compensate for the L *versus* M phase shift and appropriately set the intensity ratio of the L and M components. If these phase shifts are left uncompensated, then moving, nominally equiluminant gratings, when clearly suprathreshold, will directly stimulate the luminance mechanism.

Our analysis of the quadrature protocol showed that the detection contours will be straight despite a relative phase shift of the L and M signals. The straight contours we measured indicate that the LUM motion and flicker mechanism is reasonably additive, i.e. they respond to the linear sum of cone signals. However, Kaiser, Vimal, Cowan & Hibino (1989) tested additivity at the motion cross-over point and observed small deviations from additivity.

At the motion threshold, our low frequency (1–4 Hz) chromatic gratings often appeared to move slowly compared with equivalent luminance patterns; an effect which has been well documented (Moreland, 1982; Cavanagh *et al.* 1984; Mullen & Boulton, 1992*a*). Our psychometric functions indicated that the moving (4 Hz) red–green chromatic pattern produced essentially no motion sensation at the level at which the pattern could be detected well; similarly, a low temporal-frequency S cone grating detected by a *chromatic* mechanism may not produce a motion signal (Lee & Stromeyer, 1989). Possibly chromatic, or hue, mechanisms do not produce motion signals, and the motion signals generated by coloured patterns occur via separate mechanisms, such as SPO for the red–green patterns and LUM for the S cone patterns (Lee & Stromeyer, 1989). The apparent slowing of the chromatic gratings might be caused by interfering, masking signals from hue mechanisms that do not signal motion. Cavanagh *et al.* (1984) and Mullen & Boulton (1992*b*), for example, showed that the perceived motion of a luminance grating is slowed by adding colour contrast to the grating.

Although the LUM and SPO mechanisms can be partly separated, other work suggests that they interact at suprathreshold levels. Cavanagh & Anstis (1991) showed that a drifting equiluminant grating can cancel the motion of a luminance grating with opposite drift. Chichilnisky, Heeger & Wandell (1993) generalized this procedure, demonstrating motion nulls between oppositely drifting gratings of arbitrary spectral composition. Mullen & Baker (1985) and Derrington & Badcock (1985) observed transfer of motion after-effects between chromatic and luminance patterns. Webster & Mollon (1993) showed that adaptation to low temporal frequency gratings with combined luminance and chromatic flicker could selectively bias the motion cross-over in the quadrature protocol. On the other hand, the observations by Krauskopf & Farell (1990) on the motion coherence of chromatic plaids suggest a considerable independence between different spectral mechanisms. The grating components in the plaids had very different spatial orientations, but in the studies showing interactions, the components were parallel.

Relation to physiology

The colour-opponent, P ganglion cells and parvocellular LGN cells may underlie our RG thresholds. Lesions in the parvocellular layers severely disrupt colour detection (Schiller, Logothetis & Charles, 1990; Merigan, Katz & Maunsell, 1991). Lee, Martin & Valberg (1989*a*) observed that the typical red–green P ganglion cell, when stimulated with uniform red–green chromatic flicker, responded to the linear difference of equally weighted L and M contrast signals over the range 1–20 Hz. Derrington, Krauskopf & Lennie (1984) showed that the opponent L and M contrast weights are also approximately equal for red–green parvocellular LGN cells. Lennie, Krauskopf & Sclar (1990) observed a similar cone weighting for the non-oriented, colour-opponent cells in striate cortex, whereas for the oriented simple and complex cells, L and M inputs were typically opponent with an approximately twofold L cone contrast advantage. We observed a similar L cone advantage for the SPO motion mechanism at 2 and 4 Hz where the SPO mechanism was reasonably isolated with simple moving gratings. The foveal direction thresholds of Gegenfurtner & Hawken (1995) at 2 and 4 Hz are like ours in showing an L cone advantage in SPO. In contrast, our RG hue detection contours have slopes of ~1·0 from 1 to 15 Hz, indicating a response to the linear difference of equally weighted L and M cone contrasts. At the higher frequencies we used a hue criterion, so the results presumably reflect a chromatic mechanism and not an effect of non-linear response distortion in the phasic ganglion cells (Lee *et al.* 1989*a*; Lee, Martin & Valberg, 1989*b*).

Reid & Shapley (1992) showed that the L and M cone inputs are separately confined to the centre and surround of the red–green P cell receptive field. The surround response has a substantial lag of 1–3 deg Hz^{-1} relative to the centre as measured in all types of red–green opponent P cells (Smith, Lee, Pokorny, Martin & Valberg, 1992). Our phase measurements for RG showed a relative phase shift of L *versus* M of only ~3 deg at 9 Hz. The psychophysical judgements, however, may reflect a summated response of the various P cells, where delayed L cone surrounds and delayed M cone surrounds are about equally represented, and thus the effect of surround lag may be largely neutralized.

The phasic retinal ganglion cells apparently form the initial part of the luminance pathway for detecting rapid flicker and motion (Lee, Martin & Valberg, 1988). These cells and their magnocellular LGN target cells provide the major input to the middle temporal (MT) visual area, which is specialized for motion (Maunsell, Nealy & DePriest, 1990). Lesions in the magnocellular layers greatly reduce sensitivity to rapid flicker and motion (Schiller *et al.* 1990; Merigan, Byrne & Maunsell, 1991), although detection of slow motion is little affected, indicating that the P cell pathway can also be used to detect slow motion. We isolated the luminance mechanism, which summates L and M signals, by measuring detection contours for drifting gratings of high velocity and for quadrature patterns of low and high velocities. At low velocities, the L contrast weight was considerably greater than the M weight; at 21 Hz, the L and M weights were more alike. Lee *et al.* (1989*a*) observed similar effects in the phasic cells tested with uniform large-field flicker: at 10 Hz the L and M contrast weights were similar, but at low frequencies almost every cell showed a relatively stronger L input. Our results were obtained on adapting fields of 577 or 580 nm, and Lee *et al.* (1989*a*) used a field of rather similar chromaticity. We have also observed (Stromeyer, Lee & Eskew, 1992) a dominance of the L cones at low frequency on the 580 nm field, by measuring the LUM detection contour with a 200 ms uniform flash in peripheral retina, where colour sensitivity is low. The ratio of L' to M' weights was 2·6 and 3·6 for two observers. Gegenfurtner & Hawken (1995) isolated LUM in the parifovea by measuring direction thresholds. Their results show a greater L' weight at high temporal frequency (16 Hz) than do ours. However, their adapting field was of shorter wavelength than ours (~568 *versus* ~580 nm) and our recent observations (unpublished) show that field wavelength affects the relative L' and M' weights in LUM at different temporal frequencies.

Perhaps we would find a smaller variation in the L and M weights using a higher spatial frequency that isolates the receptive field centres (where the L and M inputs have the same sign). Lee *et al.* (1988) observed less variability in photometric flicker nulls with a small stimulus confined to the receptive field centre, and Derrington *et al.* (1984) observed that temporal frequency had little effect on the response null plane using an achromatic grating of optimal spatial frequency for the cell, which reduces the strength of the surround mechanism.

Many magnocellular cells have an antagonistic surround dominated by L cones (Reid & Shapley, 1992), like the type IV cells of Wiesel & Hubel (1966). Such surrounds would decrease sensitivity to L cone gratings at low spatial frequency and thus could not explain our results that LUM is dominated by L cones at low velocities. Smith *et al.* (1992) rejected a model of phasic cells with a simple L cone surround.

Smith *et al.* (1992) argue that at *low* temporal frequencies, the phasic cells have a surround component that is partly chromatically opponent, which, through a surround delay, introduces a large phase shift in the response to a pair of uniform, flickering red and green lights. Red light had to be advanced relative to green to get the best response, implying a lag of the L signal in the cell response. The phase shift disappeared when the flicker rate was high (20 Hz) or the flicker was confined to the receptive field centre. Our phase measurements for luminance flicker or motion also show that the L signal lags M at low and intermediate rates, and the phase shift is small near 20 Hz. Recently, we observed (Stromeyer, Chaparro, Tolias & Kronauer, 1994) that the phase shift is strongly dependent on background field colour, with the L cone signal lagging M on adapting fields longer than 570 nm (greenish-yellow) and the M signal lagging L on shorter wavelength fields (see also Swanson *et al.* 1988). The relative phase shifts reached a maximum of approximately ±70 deg at 9 Hz. Thus, in the present study, the L lag in the LUM mechanism is caused by our adapting field (577 or 580 nm) being longer than 570 nm. The physiological work, showing an L lag, was performed only on an orange field of 595 nm (Smith *et al.* 1992); other coloured adapting fields remain to be tested. The psychophysical results of Lindsey & Teller (1988) suggest that the phase shifts we observe may decrease at a higher spatial frequency, perhaps because the phasic receptive field centre is better isolated.

While our results for RG and LUM mimic properties of the tonic and phasic ganglion cells, the physiological basis of the spectrally opponent motion mechanism is less clear. SPO is unlikely to be a simple distortion in the response of phasic cells since it can be measured at contrast levels well below the luminance threshold. Gegenfurtner, Kiper, Beusmans, Carandini, Zaidi & Movshon (1994) argue that the detection of rapid (8 Hz) equiluminant patterns may be mediated by area MT, since some MT cells respond to equiluminant patterns with sensitivity comparable to thresholds measured for the behaving animal. But, at

low velocities, the animal's sensitivity to equiluminant coloured patterns is much greater than that of all measured MT cells. Thus, what we call the SPO mechanism may reflect different physiological mechanisms at low and at high velocities.

CAVANAGH, P. & ANSTIS, S. (1991). The contribution of color to motion in normal and color-deficient observers. *Vision Research* **31**, 2109–2148.

CAVANAGH, P. & FAVREAU, O. E. (1985). Color and luminance share a common motion pathway. *Vision Research* **25**, 1595–1601.

CAVANAGH, P., MACLEOD, D. I. A. & ANSTIS, S. M. (1987). Equiluminance: spatial and temporal factors and the contribution of blue-sensitive cones. *Journal of the Optical Society of America* A **4**, 1428–1438.

CAVANAGH, P., TYLER, C. W. & FAVREAU, O. E. (1984). Perceived velocity of moving chromatic gratings. *Journal of the Optical Society of America* A **1**, 893–899.

CHICHILNISKY, E.-J., HEEGER, D. & WANDELL, B. A. (1993). Functional segregation of color and motion perception examined in motion nulling. *Vision Research* **33**, 2113–2125.

COLE, G. R., STROMEYER, C. F. III & KRONAUER, R. E. (1990). Visual interactions with luminance and chromatic stimuli. *Journal of the Optical Society of America* A **7**, 128–140.

DERRINGTON, A. M. & BADCOCK, D. R. (1985). The low level motion system has both chromatic and luminance inputs. *Vision Research* **25**, 1879–1884.

DERRINGTON, A. M. & HENNING, G. B. (1993). Detecting and discriminating the direction of motion of luminance and colour gratings. *Vision Research* **33**, 799–811.

DERRINGTON, A. M., KRAUSKOPF, J. & LENNIE, P. (1984). Chromatic mechanisms in lateral geniculate nucleus of macaque. *Journal of Physiology* **357**, 241–265.

GEGENFURTNER, K. R. & HAWKEN, M. J. (1995). Temporal and chromatic properties of motion mechanisms. *Vision Research* (in the Press).

GEGENFURTNER, K. R., KIPER, D. C., BEUSMANS, J. M. H., CARANDINI, M., ZAIDI, Q. & MOVSHON, J. A. (1994). Chromatic properties in macaque MT. *Visual Neuroscience* **22**, 455–466.

KAISER, P. K., VIMAL, R. L. P., COWAN, W. B. & HIBINO, H. (1989). Nulling of apparent motion as a method for assessing sensation luminance: an additivity test. *Color Research and Application* **14**, 187–191.

KRAUSKOPF, J. & FARELL, B. (1990). Influence of colour on the perception of coherent motion. *Nature* **348**, 328–331.

LEE, B. B., MARTIN, P. R. & VALBERG, A. (1988). The physiological basis of heterochromatic flicker photometry demonstrated in the ganglion cells of the macaque retina. *Journal of Physiology* **404**, 323–347.

LEE, B. B., MARTIN, P. R. & VALBERG, A. (1989*a*). Sensitivity of macaque retinal ganglion cells to chromatic and luminance flicker. *Journal of Physiology* **414**, 223–243.

LEE, B. B., MARTIN, P. R. & VALBERG, A. (1989*b*). Nonlinear summation of M- and L-cone inputs to phasic retinal ganglion cells of the macaque. *Journal of Neuroscience* **9**, 1433–1442.

LEE, J. & STROMEYER, C. F. III (1989). Contribution of human short-wave cones to luminance and motion detection. *Journal of Physiology* **413**, 563–593.

LENNIE, P., KRAUSKOPF, J. & SCLAR, G. (1990). Chromatic mechanisms in striate cortex of macaque. *Journal of Neuroscience* **10**, 649–669.

LINDSEY, D. T., POKORNY, J. & SMITH, V. C. (1986). Phase-dependent sensitivity of heterochromatic flicker. *Journal of the Optical Society of America* A **3**, 921–927.

LINDSEY, D. T. & TELLER, D. Y. (1988). Spatio-temporal phase characteristics of moving gratings synthesized from isoluminant red and green components. *Investigative Ophthalmology and Visual Science* **29**, 302.

LINDSEY, D. T. & TELLER, D. Y. (1990). Motion at isoluminance: discrimination/detection ratios for moving isoluminant gratings. *Vision Research* **30**, 1751–1761.

LIVINGSTONE, M. S. & HUBEL, D. H. (1987). Psychophysical evidence for separate channels for the perception of form, color, movement, and depth. *Journal of Neuroscience* **7**, 3416–3468.

MAUNSELL, J. H. R., NEALY, T. A. & DEPRIEST, D. D. (1990). Magnocellular and parvocellular contributions to responses in the middle temporal visual area (MT) of the macaque monkey. *Journal of Neuroscience* **10**, 3323–3334.

MERIGAN, W. H., BYRNE, C. E. & MAUNSELL, J. H. R. (1991). Does primate motion perception depend on the magnocellular pathway? *Journal of Neuroscience* **11**, 3422–3429.

MERIGAN, W. H., KATZ, L. M. & MAUNSELL, J. H. R. (1991). The effects of parvocellular lateral geniculate lesions on the acuity and contrast sensitivity of macaque monkeys. *Journal of Neuroscience* **11**, 994–1001.

METHA, A. B., VINGRYS, A. J. & BADCOCK, D. R. (1994). Detection and discrimination of moving stimuli: the effects of color, luminance, and eccentricity. *Journal of the Optical Society of America* A **11**, 1697–1709.

MORELAND, J. D. (1982). Spectral sensitivity by motion photometry. In *Documenta Ophthalmologica Proceedings Series*, vol. 33, ed. VERRIEST, G., pp. 61–66. Dr W. Junk Publishers, The Hague.

MULLEN, K. T. & BAKER, C. L. JR (1985). A motion aftereffect from an isoluminant stimulus. *Vision Research* **25**, 685–688.

MULLEN, K. T. & BOULTON, J. C. (1992*a*). Absence of smooth motion perception in color vision. *Vision Research* **32**, 483–488.

MULLEN, K. T. & BOULTON, J. C. (1992*b*). Interactions between colour and luminance contrast in the perception of motion. *Ophthalmology and Physiological Optics* **12**, 201–205.

PALMER, J., MOBLEY, L. A. & TELLER, D. Y. (1993). Motion at isoluminance: discrimination/detection ratios and the summation of luminance and chromatic signals. *Journal of the Optical Society of America* A **10**, 1353–1362.

POWELL, I. (1981). Lens for correcting chromatic aberration of the eye. *Applied Optics* **20**, 4152–4155.

RAMACHANDRAN, V. S. & GREGORY, R. L. (1978). Does colour provide an input to human motion perception? *Nature* **275**, 55–56.

REID, R. C. & SHAPLEY, R. M. (1992). Spatial structure of cone inputs to receptive fields in primate lateral geniculate nucleus. *Nature* **356**, 716–718.

SCHILLER, P. H., LOGOTHETIS, N. K. & CHARLES, E. R. (1990). Role of the color-opponent and broad-band channels in vision. *Visual Neuroscience* **5**, 321–346.

SMITH, V. C., LEE, B. B., POKORNY, J., MARTIN, P. R. & VALBERG, A. (1992). Responses of macaque ganglion cells to the relative phase of heterochromatically modulated lights. *Journal of Physiology* **458**, 191–221.

SMITH, V. C. & POKORNY, J. (1975). Spectral sensitivity of the foveal cone photopigments between 400 and 500 nm. *Vision Research* **15**, 161–171.

STROMEYER, C. F. III, CHAPARRO, A., TOLIAS, A. & KRONAUER, R. E. (1994). Colored fields produce large L vs M phase shifts in luminance motion mechanism. *Investigative Ophthalmology and Visual Science* **35**, 1644.

STROMEYER, C. F. III, COLE, G. R. & KRONAUER, R. E. (1985). Second-site adaptation in the red-green chromatic pathways. *Vision Research* **25**, 219–237.

STROMEYER, C. F. III, COLE, G. R. & KRONAUER, R. E. (1987). Chromatic suppression of cone inputs to the luminance flicker mechanism. *Vision Research* **27**, 1113–1137.

STROMEYER, C. F. III, ESKEW, R. T. JR & KRONAUER, R. E. (1990). The most sensitive motion detectors in humans are spectrally-opponent. *Investigative Ophthalmology and Visual Science* **31**, 240.

STROMEYER, C. F. III, ESKEW, R. T. JR, KRONAUER, R. E. & SPILLMANN, L. (1991*a*). Temporal phase response of the short-wave cone signal for color and luminance. *Vision Research* **31**, 787–803.

STROMEYER, C. F. III, ESKEW, R. T. JR, RYU, A. & KRONAUER, R. E. (1991*b*). Separation of luminance and spectrally-opponent motion mechanisms with a quadrature-pedestal paradigm. *Investigative Ophthalmology and Visual Science* **32**, 1094.

STROMEYER, C. F. III, KRONAUER, R. E., MADSEN, J. C. & KLEIN, S. A. (1984). Opponent-movement mechanisms in human vision. *Journal of the Optical Society of America* A **1**, 876–884.

STROMEYER, C. F. III, LEE, J. & ESKEW, R. T. JR (1992). Peripheral chromatic sensitivity for flashes: a post-receptoral red-green asymmetry. *Vision Research* **32**, 1865–1873.

SWANSON, W. H., POKORNY, J. & SMITH, V. C. (1988). Effects of chromatic adaptation on phase-dependent sensitivity to heterochromatic flicker. *Journal of the Optical Society of America* A **5**, 1976–1982.

THORNTON, J. E. & PUGH, E. N. JR (1983). Red/green color opponency at detection threshold. *Science* **219**, 191–193.

WATSON, A. B., THOMPSON, P. G., MURPHY, B. J. & NACHMIAS, J. (1980). Summation and discrimination of gratings moving in opposite directions. *Vision Research* **20**, 341–347.

WEBSTER, M. A. & MOLLON, J. D. (1993). Contrast adaptation dissociates different measures of luminous efficiency. *Journal of the Optical Society of America* A **10**, 1332–1340.

WETHERILL, G. B. (1963). Sequential estimation of quantal response curves. *Journal of the Royal Statistical Society* B **25**, 1–48.

WIESEL, T. N. & HUBEL, D. H. (1966). Spatial and chromatic interactions in the lateral geniculate body of the rhesus monkey. *Journal of Neurophysiology* **29**, 1115–1156.

Acknowledgements

This research was supported by NIH-01808, AFOSR 86-0338 and the Milton Fund. We are grateful to Dr J. G. Daugman for helping with the electronics and Dr A. M. Derrington for comments on the paper.

Received 19 April 1994; accepted 31 October 1994.